Columnar aerosol optical properties at AERONET sites in central eastern Asia and aerosol transport to the tropical mid-Pacific

T. F. Eck,[1,2] B. N. Holben,[2] O. Dubovik,[1,2] A. Smirnov,[1,2] P. Goloub,[3] H. B. Chen,[4] B. Chatenet,[5] L. Gomes,[6] X.-Y. Zhang,[7] S.-C. Tsay,[8] Q. Ji,[8,9] D. Giles,[2,9] and I. Slutsker[2,9]

Received 23 July 2004; revised 9 November 2004; accepted 7 January 2005; published 18 March 2005.

[1] The column-integrated optical properties of aerosol in the central eastern region of Asia and midtropical Pacific were investigated based on Sun/sky radiometer measurements made at Aerosol Robotic Network (AERONET) sites in these regions. Characterization of aerosol properties in the Asian region is important due to the rapid growth of both population and economic activity, with associated increases in fossil fuel combustion, and the possible regional and global climatic impacts of related aerosol emissions. Multiyear monitoring over the complete annual cycle at sites in China, Mongolia, South Korea, and Japan suggest spring and/or summer maximum in aerosol optical depth (τ_a) and a winter minimum; however, more monitoring is needed to establish accurate climatologies. The annual cycle of Angstrom wavelength exponent (α) showed a springtime minimum associated with dust storm activity; however, the monthly mean $\alpha_{440-870}$ was >0.8 even for the peak dust season at eastern Asian sites suggesting that fine mode pollution aerosol emitted from population centers in eastern Asia dominates the monthly aerosol optical influence even in spring as pollution aerosol mixes with coarse mode dust originating in western source regions. Aerosol optical depth peaks in spring in the tropical mid-Pacific Ocean associated with seasonal shifts in atmospheric transport from Asia, and ~35% of the springtime τ_{a500} enhancement occurs at altitudes above 3.4 km. For predominately fine mode aerosol pollution cases, the average midvisible (~550 nm) single scattering albedo (ω_0) at two continental urban sites in China averaged ~0.89, while it was significantly higher, ~0.93, at two relatively rural coastal sites in South Korea and Japan. Differences in fine mode absorption between these regions may result from a combination of factors including aerosol aging during transport, relative humidity differences, sea salt at coastal sites, and fuel type and combustion differences in the two regions. For cases where τ_a was predominately coarse mode dust aerosol in the spring of 2001, the absorption was greater in eastern Asia compared to the source regions, with ω_0 at Dunhuang, China (near to the major Taklamakan dust source), ~0.04 higher than at Beijing at all wavelengths, and Anmyon, South Korea, showing an intermediate level of absorption. Possible reasons for differences in dust absorption magnitude include interactions between dust and fine mode pollution aerosol and also variability of dust optical properties from different source regions in China and Mongolia.

Citation: Eck, T. F., et al. (2005), Columnar aerosol optical properties at AERONET sites in central eastern Asia and aerosol transport to the tropical mid-Pacific, *J. Geophys. Res.*, *110*, D06202, doi:10.1029/2004JD005274.

1. Introduction

[2] Atmospheric aerosol concentrations and their optical properties are one of the largest sources of uncertainty in current assessments and predictions of global climatic change [*Intergovernmental Panel on Climate Change* (*IPCC*), 2001; *Hansen et al.*, 2000]. Aerosol interactions result in both direct radiative forcing and indirect effects on clouds (droplet properties, cloud dynamics and lifetimes).

[1]Goddard Earth Sciences and Technology Center, University of Maryland-Baltimore County, Baltimore, Maryland, USA.
[2]Biospheric Sciences Branch, NASA Goddard Space Flight Center, Greenbelt, Maryland, USA.
[3]Laboratoire d'Optique Amosphérique, Université des Sciences et Technologies de Lille, Villeneuve d'Ascq, France.
[4]Institute of Atmospheric Physics, Chinese Academy of Sciences, Beijing, China.
[5]Laboratoire Interuniversitaire des Systèmes Atmosphériques (LISA), Université Paris, Creteil, France.
[6]CNRS, Metéo-France/CNRM/GMEI/MNPCA, Toulouse, France.
[7]Institute of Earth Environment, Chinese Academy of Sciences, XiAn, China.
[8]Climate and Radiation Branch, NASA Goddard Space Flight Center, Greenbelt, Maryland, USA.
[9]Science Systems and Applications, Inc., Lanham, Maryland, USA.

Copyright 2005 by the American Geophysical Union.
0148-0227/05/2004JD005274

Direct radiative forcings from aerosols are primarily a function of aerosol concentration in the total atmospheric column (aerosol optical depth), particle size distributions, and aerosol absorption properties. Satellite remote sensing techniques are beginning to provide more detailed information on the global distribution and dynamics of aerosol optical depth and also an estimate of the relative magnitude of fine mode versus coarse mode particles [*Kaufman et al.*, 2002; *King et al.*, 1999]. As most fine mode particles are anthropogenic in origin (primarily from fossil fuel combustion and agricultural biomass burning) and most coarse mode particles originate from natural sources (sea salt, airborne desert dust), this breakdown provides some measure of the anthropogenic contribution to the total aerosol burden. Exceptions to this simple categorization exist however as, for example, some natural aeolian desert dust is fine mode size and some fossil fuel combustion aerosols are coarse mode size, such as fly ash from coal combustion.

[3] However, satellite data does not provide complete characterization of aerosol optical properties, and information on aerosol absorption in particular is very difficult to derive from satellite remote sensing. Accurate knowledge of aerosol absorption magnitude is required for the assessment of both direct radiative forcing at the top of the atmosphere and at the Earth's surface [*Satheesh and Ramanathan*, 2000]. Additionally aerosol absorption information is critical in investigating the aerosol semidirect effect [*Hansen et al.*, 1997] whereby absorbing aerosols modify the surface and aerosol layer heating rates and therefore change the stability of the atmosphere and potentially alter the formation (or lifetime) of convective cumulus clouds [*Koren et al.*, 2004; *Ackerman et al.*, 2000]. On an even larger regional scale, simulations by *Menon et al.* [2002] suggest that absorbing aerosols in China may be responsible in part for the trend of increasing drought in northern China and increasing floods in southern China in recent decades. They suggest that the large-scale circulation and therefore hydrological cycle may be modified by the aerosol absorption that affects stability and vertical air motion. However, their study assumed highly absorbing aerosols in China, although very limited data on absorption are available in this region, and therefore the magnitude of the actual absorption is uncertain.

[4] Due to combined influences of arid dust production regions, large regional populations, and increasing fossil fuel usage, the East Asian region often experiences very high concentrations of tropospheric aerosols. This aerosol burden may increase in the future as both population and economic activity (and associated increases in fossil fuel usage) continue to grow. Estimates by *Wolf and Hidy* [1997] suggest that total particulate mass produced by China may increase by a factor of two to four (for a range of low to high fossil fuel energy consumption scenarios) over 1990 levels by the year 2040. In addition to the affects that these aerosols may have on regional climate forcings, possible reductions in crop productivity [*Chameides et al.*, 1999] and the health effects of aerosols on inhabitants of the region (and of megacities such as Beijing in particular) are also major issues of concern.

[5] The Asian Pacific Regional Aerosol Characterization Experiment (ACE-Asia) field campaign was conducted primarily in South Korea, Japan, China, and adjacent oceanic regions from late March through May 2001 to characterize the complex aerosol mixtures (pollution and dust) that occur there [*Huebert et al.*, 2003]. Spring is the peak dust production time of year, with the spring (March–May) of 2001 being a season of unusually heavy dust concentrations. The Aerosol Robotic Network (AERONET) site observations for this same region, presented in this investigation, cover the entire yearly cycle (including spring 2001 at some sites), therefore placing the aerosol characteristics and concentrations of the spring season in perspective within the annual cycle. One of the aerosol parameters that AERONET measurements and analysis provide is an estimate of column integrated aerosol absorption as parameterized by the spectral single scattering albedo (ω_0). *Nakajima et al.* [2003] emphasized that for the east China Sea region the springtime aerosol direct radiative forcing was highly dependent on the single scattering albedo, resulting in forcing differences of ~40% due to differing estimates of ω_0 obtained from measurements and models. In addition to data from AERONET sites in China, Mongolia, Korea, and Japan, we also analyze data from three sites in the Hawaiian Islands in this study, in order to investigate the long-range transport of aerosols in spring to the tropical mid-Pacific.

2. Study Region, Instrumentation, and Methodology

2.1. Region of Study

[6] Maps showing the locations of the AERONET Sun-sky radiometers utilized in this study are shown in Figures 1a and 1b. We present results from multiyear monitoring at four Asian sites: Dalanzadgad, Mongolia; Beijing, China; Anmyon Island, South Korea; and Shirahama, Japan. In addition, data from 2001 for ~2 months from Dunhuang, China and for ~7 months in 2002 from Yulin, China are also analyzed. Data from XiangHe, China for ~1 month are also presented, however this site is not shown on the Figure 1a map since it is very close to Beijing, only ~80 km to the east-southeast. These sites span a wide range of environments ranging from arid continental locations in China and Mongolia to a coastal Pacific Ocean location in Japan. In addition to these Asian sites, we also analyze data from three sites in the Hawaiian Island chain to investigate the spring season transport of aerosols from Asia to the tropical and subtropical mid-Pacific. Results of multiyear monitoring at Mauna Loa Observatory at 3.4 km altitude on the island of Hawaii and from Lanai at a location near sea level are shown. Additionally data for ~1 year, 2001, are given for Midway Island at near sea level, in the far Northwest Hawaiian islands. Notably, three of the sites studied in this paper, Anmyon Island, Mauna Loa Observatory, and Midway have been proposed as monitoring sites for the Atmospheric Brown Cloud (ABC) network [*Ramanathan and Crutzen*, 2003]. Goals of the ABC project in the Asian and Pacific region include the characterization of aerosol sources and species, aerosol-cloud interactions, and the effect of aerosols on the radiation budget in the region.

2.2. Instrumentation

[7] All of the CIMEL Electronique CE-318 Sun-sky radiometer measurements reported in this paper were made with instruments that are a part of the AERONET global

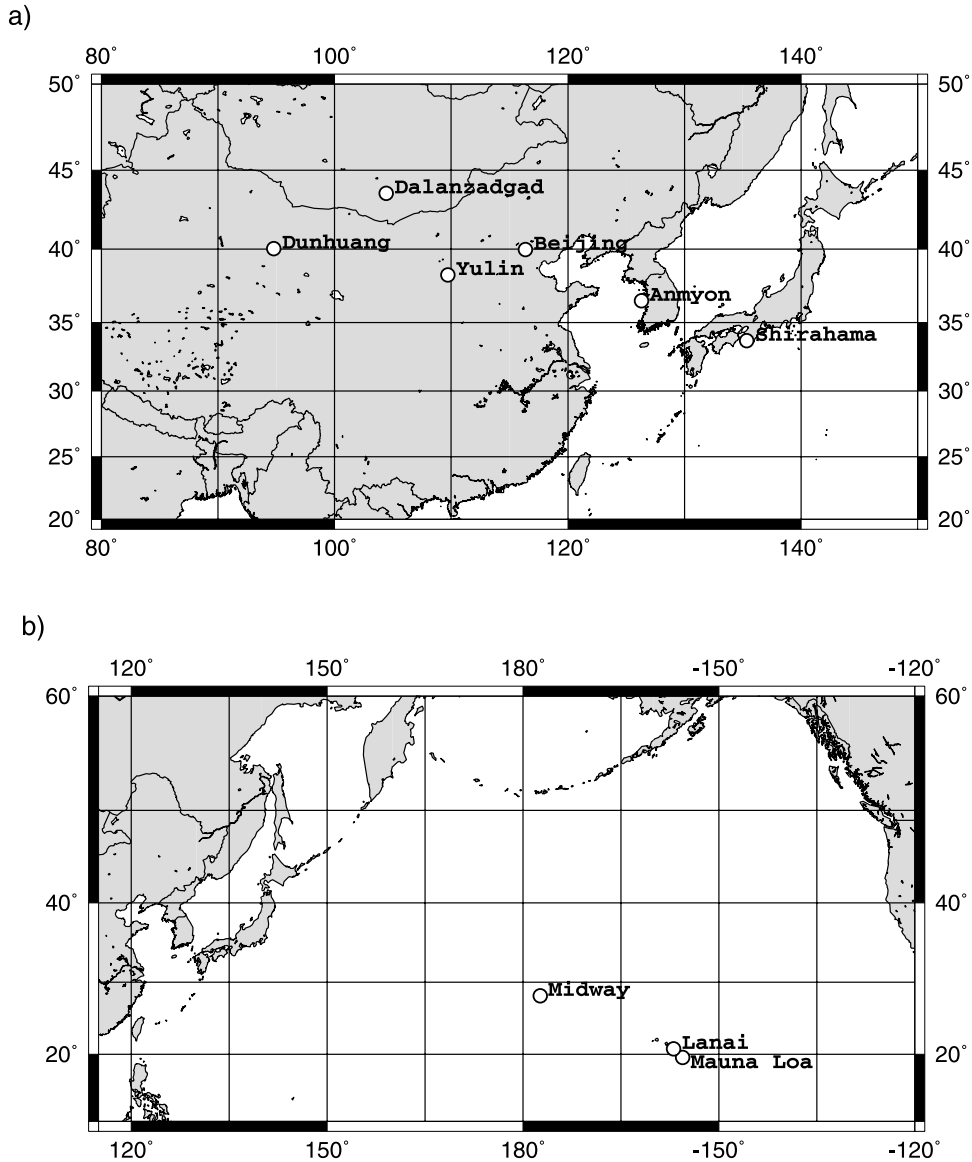

Figure 1. (a) Map of the Asian region studied with the location of AERONET sites that were monitored for differing time intervals during the 1999–2003 time period. (b) Map of the Pacific Ocean region showing the three Hawaiian Island sites analyzed in this study.

network. These instruments are described in detail in *Holben et al.* [1998]; however, a brief description will be given here. The automatic tracking Sun and sky scanning radiometers made direct Sun measurements with a 1.2° full field of view every 15 min at 340, 380, 440, 500, 675, 870, 940, and 1020 nm (nominal wavelengths). However, for both Yulin and Beijing (2002 and 2003 only) the polarized version of the CIMEL made measurements at 440, 675, 870, 940, and 1020 nm, in addition to three polarized channels at 870 nm (not analyzed in this study). The direct Sun measurements take ~8 seconds to scan all 8 wavelengths, with a motor driven filter wheel positioning each filter in front of the detector. These solar extinction measurements are then used to compute aerosol optical depth at each wavelength except for the 940 nm channel, which is used to retrieve total precipitable water in centimeters. The filters utilized in these instruments were ion assisted deposition interference filters with band pass (full width at half maximum) of 10 nm except for the 340 nm channel at 2 nm and the 380 nm filter at 4 nm. Calibration of field instruments was performed by a transfer of calibration from reference instruments which were calibrated by the Langley plot technique at Mauna Loa Observatory (MLO), Hawaii. The intercalibration of field instruments was performed both predeployment and postdeployment at Goddard Space Flight Center (GSFC), and a linear change in calibration with time was assumed in the interpolation between the two calibrations. The combined effects of uncertainties in calibration, atmospheric pressure (not monitored), and total ozone amount (climatology is used) result in a total uncertainty of ~0.010–0.021 in computed τ_a for field instruments (which is spectrally dependent with the higher errors in the UV [*Eck et al.*, 1999]). *Schmid et al.* [1999] compared τ_a values derived from 4 different solar radiometers (one

was an AERONET Sun-sky radiometer) operating simultaneously together in a field experiment and found that the τ_a values from 380 to 1020 nm agreed to within 0.015 (rms), which is similar to our estimated level of uncertainty in τ_a retrieval for field instruments. The spectral aerosol optical depth data have been screened for clouds, following the methodology of *Smirnov et al.* [2000], which relies on the greater temporal variance of cloud optical depth versus aerosol optical depth. The sky radiances measured by the Sun/sky radiometers are calibrated versus the 2-meter integrating sphere at the NASA Goddard Space Flight Center, to an absolute accuracy of ~5% or less.

2.3. Analysis Methodology

[8] The CIMEL sky radiance almucantar measurements at 440, 675, 870, and 1020 nm (nominal wavelengths) in conjunction with the direct Sun measured τ_a at these same wavelengths were used to retrieve aerosol size distributions following the methodology of *Dubovik and King* [2000]. Almucantar sky radiance measurements were made at optical air masses of 4, 3, and 2 in the morning and afternoon, and once per hour in between. Only almucantar scans at solar zenith angles greater than 45 degrees are analyzed and presented here, in order to insure sky radiance data over a wide range of scattering angles. Spheroid particle shape was assumed in the retrievals since coarse mode aerosol was often present in the aerosol mixtures especially in spring, which is the peak season of strong desert dust events. Use of the spheroid particle shape assumption with a fixed aspect ratio distribution [*Dubovik et al.*, 2002b] minimized artifacts in size distribution retrievals that result from nonspherical particle scattering. Further discussion of the spheroid shape assumption retrievals and comparisons of both size distribution and single scattering albedo retrievals made with spherical versus spheroid shape assumptions are given in sections 3.2 and 3.3. In order to eliminate cloud contamination from the almucantar directional sky radiance data we require the radiances to be symmetrical on both sides of the Sun at equal scattering angles. We eliminated scattering angle radiance pairs that are not symmetrical and required that a minimum of 21 angles remain out of a maximum total of 27 angles. Sensitivity studies performed by *Dubovik et al.* [2000] were used to analyze the perturbations of the inversion resulting from random errors, possible instrument offsets and known uncertainties in the atmospheric radiation model. Retrieval tests using known size distributions demonstrated successful retrievals of mode radii and the relative magnitude of modes for various types of size distributions such as bimodal accumulation mode dominated aerosols and bimodal coarse mode dominated aerosols. Simultaneous retrievals of aerosol single scattering albedo are also made with this algorithm and the sensitivity analysis shows that these retrievals have an uncertainty of ~0.03 for both desert dust and biomass burning aerosols when $\tau_{a440} \geq 0.5$ [*Dubovik et al.*, 2000].

3. Column Integrated Aerosol Optical Properties

[9] The radiation fields that the Sun/sky radiometers measure of the spectral and directional sky radiances and the direct Sun optical depth are determined by the aerosol size distributions and complex refractive indices of the entire atmospheric column. Therefore the retrieval by AERONET of aerosol parameters such as the single scattering albedo, size distribution, and refractive indices are the radiatively effective column integrated values of these parameters. As a result, these remotely sensed parameters may differ from in situ measurements made at the surface or at various altitudes by aircraft-based instruments. Measurements made by airborne Sun photometers during ACE-Asia [*Schmid et al.*, 2003; *Redemann et al.*, 2003] in spring of 2001 in the vicinity Japan and South Korea show that not only were the aerosols often stratified in distinct horizontal layers but these layers were at times composed of different aerosol types and size distributions, with high altitude dust layers (up to 10 km altitude) sometimes overlying pollution aerosol in the boundary layer. *Seinfeld et al.* [2004] synthesize other measurements of aerosol vertical distributions made from lidar and aircraft in situ sampling during ACE-Asia and modeled vertical distributions. These varied vertical profiles and mixing of aerosol types lead to both complex radiative effects and complex chemical interactions from mineral dust and pollution interaction.

[10] Nevertheless, the remotely sensed column-integrated aerosol parameters retrieved from AERONET measurements provide valuable information on the aerosol column effects on radiative forcing that is important in assessing aerosol influence on regional climate [*Conant et al.*, 2003] and for application to retrieval of aerosol from satellite radiance measurements [*Kaufman et al.*, 2002].

3.1. Aerosol Optical Depth

[11] A comparison of monthly mean aerosol optical depth (τ_a) at 500 nm for the five principal Asian sites of this study is shown in Figure 2a. The measurements are not coincident for the same time periods since for one site less than a single year of data exits (e.g., Yulin, China in 2002) while other sites have a multiyear average record (e.g., Dalanzadgad, Mongolia 1997–2003 and Shirahama, Japan 2001–2004). Nevertheless, this comparison shows the general magnitude and in some cases (where multiyear data are available) the seasonality of τ_{a500}. Multiyear averages are necessary in order to characterize a truly representative climatological seasonal cycle. For example, the large τ_{a500} jump at Anmyon in June seems unlikely to be a typical annual feature, especially since there is only one year of data (2001) for this month while most other months for Anmyon are averages of 2 to 3 years (except July and August which are also only 2001 data). Figure 2a shows large regional differences in aerosol concentration are evident, with the highest τ_{a500} in the city of Beijing (~2 years of data), with monthly means ranging from ~0.40 to 1.10. At the other extreme, the τ_{a500} at Dalanzadgad in the Gobi desert of southern Mongolia remains relatively low all year with a monthly maximum of 0.20 in May and minimum of ~0.05 to 0.06 (clean background levels) in December and January. However, *Kim et al.* [2004] measured τ_{a500} by Sun photometer at Mandalgovi, Mongolia (~275 km to the north-northeast of Dalanzadgad) to be much higher, with a long-term yearly mean of ~0.40 compared to a yearly mean of 0.12 at Dalanzadgad. This very large difference in τ_{a500} over a relatively small distance suggests possible strong local aerosol sources within Mongolia (both sites

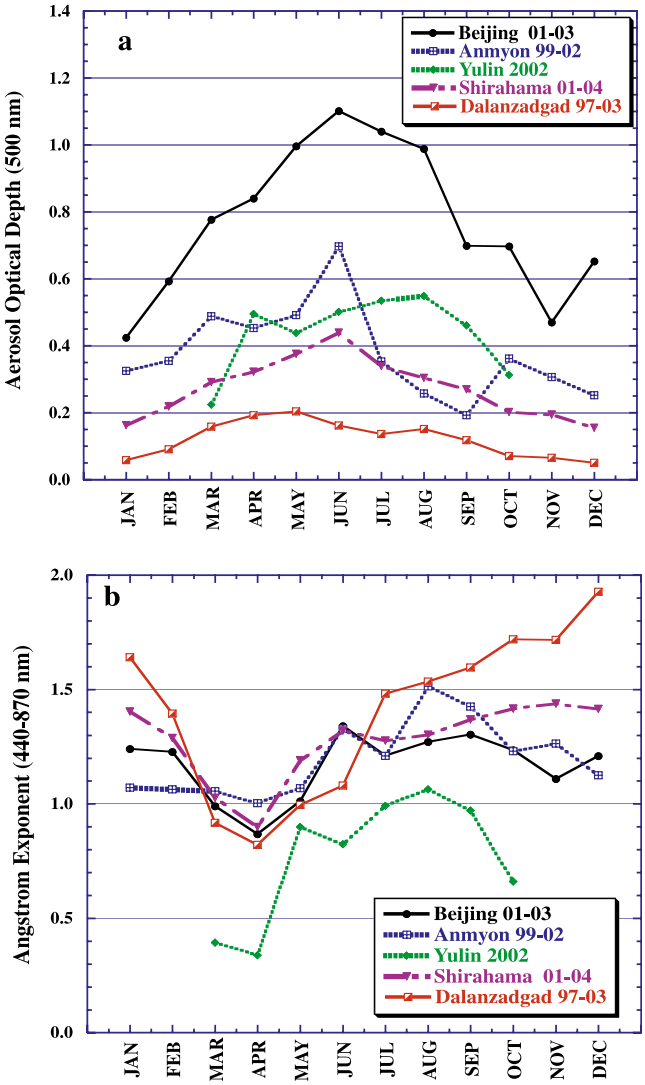

Figure 2. (a) Monthly means of τ_{a500} for the five principal Asian sites analyzed in this study. Note that time intervals differ for each site, with one site (Dalanzadgad) having ~6 years of data, while another site (Yulin) only has data from one year, 2002. (b) Monthly average Angstrom wavelength exponents (computed from linear regression of ln τ_a versus ln λ with 440, 500, 675, and 870 nm data; $\alpha_{440-870}$) for the same data as shown in Figure 2a.

have small populations of ~14,000 each), and the reasons for this difference should be investigated. The other three AERONET sites in Figure 2a (Anmyon, Yulin, and Shirahama) all show moderate to large enhancements in τ_{a500} well above the background aerosol level in nearly all months. Interestingly, the peak monthly mean τ_{a500} occurs in June at three sites, Beijing, Anmyon, and Shirahama; however, additional monitoring is necessary to establish if this is a persistent feature in the annual cycle of the region. It is noted that biomass burning aerosols (often at very high optical depth), from extensive forest fires in the Lake Baikal region of Siberia, were observed at the Beijing and Dalanzadgad sites in the spring and early summer of 2003. *Aoki and Fujiyoshi* [2003] present multiyear seasonal means of τ_{a500} from sky radiometer measurements at four stations in Japan at midlatitudes (ranging from 36° to 43°N). They found maximum seasonal mean τ_{a500} in spring at all four sites, summer showing the second highest values, and lowest seasonal means in winter for two stations and in fall for the other two stations. The overall seasonal minimum τ_{a500} for all four stations was 0.18 in winter and the maximum was 0.44 in spring.

[12] It is interesting that the seasonal cycle of column total aerosol optical depth that we have measured by Sun photometry at these AERONET sites differs from the seasonal variation of aerosol concentrations observed by ground based in situ sampling of aerosol in the region. For example, *Chen et al.* [1997] measured the chemical composition of aerosols in Cheju Island, South Korea (a rural site) from daily samples over a 3-year period and found the highest concentrations of sea salt in winter, most other species peaking in spring and a pronounced minimum for all species in summer. In the megacity of Seoul, South Korea, *Lee et al.* [1999] measured total particulate matter with diameter less than 2.5 μm ($PM_{2.5}$) near ground level and found maximum concentrations in winter and minimum in summer, with data collected on 12–15 days per season. Possible reasons for seasonal differences between total column optical depth and surface concentrations in this region include seasonal variation of the aerosol altitudinal profile, seasonal variation in atmospheric relative humidity vertical profiles, and seasonal variability of rainfall and cloud cover. The boundary layer (which is often the dominant aerosol layer) is likely deeper in summer, due to stronger convective mixing resulting from stronger solar heating, possibly resulting in lower surface concentrations and yet greater column loadings. Additionally, both total column integrated water vapor and surface relative humidity (RH) are maximum in summer and minimum in winter. This results in greater hygroscopic aerosol growth in summer at higher relative humidity and may affect optical extinction greater than surface mass concentrations, especially if the RH and hygroscopic growth is greater for layers above the surface. Also, since Sun photometer measurements can be made only for meteorological conditions that result in low cloud cover or where the Sun is visible in cloud gaps, these measurements are naturally biased towards atmospheric high-pressure systems. Therefore there are relatively few measurements taken during cloudy and rainy periods, and in this region the summer months experience the maximum rainfall and cloud cover. It is likely that ground level in situ sampling done on rainy days would record lower aerosol concentrations due to washout and wet deposition of aerosols and that this may result in lower seasonal mean concentrations during months of higher rainfall. It would be valuable to study the relationships between daily and seasonal total column aerosol optical depth and surface concentrations at a site with both of these measurement types in addition to lidar (for aerosol profiles) and relative humidity soundings; however, this is beyond the scope of this investigation.

[13] Aerosol optical depth at 750 nm, for several sites in China, has been estimated by *Qiu* [2003] from broadband direct solar radiation data measured by pyrheliometers (spectral range 300 to 4000 nm). For Beijing, the eight-year long-term (1993–2000) mean τ_a at 750 nm is 0.512 as

estimated from hourly pyrheliometer data [*Qiu*, 2003]. Estimated yearly mean τ_a at 500 nm from this data is 0.77, as computed from the Angstrom exponent equal to 1.0, the value that is assumed in the pyrheliometer retrievals. This result is exactly equal to the 2-year mean of τ_{a500} at Beijing from the AERONET Sun photometer data for 2002–2003. Although the years differ, thus not a direct comparison, and the yearly mean Angstrom exponent from AERONET is 1.17 for Beijing (not 1.0 as assumed), this agreement suggests that the algorithm of *Qiu* [2003] provides reasonable estimates of τ_a from the pyrheliometer instrument network. *Xia et al.* [2005] compared hourly average τ_{a750} from Beijing pyrheliometer data processed by the method of *Qiu* [2003] to AERONET estimates at 750 nm for the Beijing region (sites ~50 km apart) in April 2001. They found good agreement, with high correlation (r = 0.93) and mean τ_{a750} of 0.42 from AERONET and 0.45 from the pyrheliometer data for April 2001. Monthly mean τ_{a750} at Beijing for one year (1995) from pyrheliometer retrievals [*Qiu*, 2003] show a maximum value in July with June and April being the next highest, while the lowest monthly means occurred in December and January. This annual trend in monthly mean τ_a at Beijing is similar to that measured at the AERONET site in 2002–2003 (Figure 2a), therefore providing further evidence for a summer maximum and winter minimum at this site.

[14] The monthly mean Angstrom exponents (α) for the five principal sites are shown in Figure 2b, corresponding to the same observations as the τ_{a500} data shown in Figure 2a. These α values are computed from linear regression of ln τ_a versus ln λ with data from 440, 500, 675, and 870 nm (except for Beijing and Yulin where the polarized version of the Cimel Sun/sky radiometer does not include the 500 nm channel). A common feature at all sites is the local minimum in spring (March through May) due to the influence of coarse mode desert dust aerosols in this season [*Takemura et al.*, 2003]. The seasonality of $\alpha_{440-870}$ is particularly pronounced in Dalanzadgad which is located in an arid region where dust is generated in the spring, but not in large concentrations. However, the minimum value of α at Dalanzadgad is 0.82 in April, which suggests that even during the peak desert dust month the fine mode aerosol component make a significant contribution to the total optical depth. The α values in Yulin in 2002 were lower than all the other sites in most months, since Yulin is located in an arid environment which is immediately to the east of more active dust production regions. Therefore coarse mode desert dust is a more persistent feature at this site, with dust clearly dominating the τ_a in March and April (α = 0.39). This compares with a mean $\alpha_{450-700}$ value of 0.53 (±0.45) measured at ground level near Yulin in April 2002 by a 3 wavelength integrating nephelometer as reported in *Alfaro et al.* [2003]. The ground-based nephelometer measured α is higher than that given by the Sun photometer since dust is often present above a ground-level pollution or mixed aerosol layer.

[15] The average Angstrom exponents in all months do not exceed ~1.5 for any of the sites except for Dalanzadgad. These α values of ~1.0 to 1.5 for Anmyon, Beijing, and Shirahama imply that aerosol mixtures of both coarse and fine mode particles predominate in this region and also reflect the occurrence of large size accumulation mode particles that may result from fine particle coagulation at high concentrations and from hygroscopic growth (see section 3.2). For comparison, regions that are dominated by fine mode pollution only (from fossil fuel combustion and industrial activity) such as the U.S. mid-Atlantic region AERONET site at GSFC (in Greenbelt, Maryland) show monthly mean α for most months >1.7 [*Holben et al.*, 2001]. Similarly, biomass burning in Brazil and southern African sites also show monthly mean α > 1.7 in burning season months. *Anderson et al.* [2003] observed during the ACE-Asia experiment, from in situ aircraft sampling near South Korea and Japan, that the pollution aerosol sampled always appeared to have a significant coarse mode present, suggesting that the coarse mode is co-emitted with the fine mode pollution particles. These observations in general are consistent with our AERONET measurements in Beijing, Anmyon, and Shirahama. The only site of our 5 Asian AERONET sites presented here that has significantly higher α than 1.5 is Dalanzadgad, and these high values occur during the months of September through January when monthly average τ_{a500} is low, ranging from 0.05 to 0.12. These high α values that occur in fall and winter in Mongolia may possibly result from the combined influences of local coal burning for cooking and heating, pollution transport from cities and oil field gas flaring in Siberia to the north and northwest, and also possibly from pollution advected from Europe.

[16] Except for Yulin, the lowest monthly mean α at the other 4 sites are >0.80 which suggests that even though coarse mode aerosols are typically present in this region, it is the fine mode submicron radius particles that dominate the optical depth in all seasons (further discussion in section 3.2). Sun photometer measurements made at two sites on Honshu Island, Japan in March and April 2002 [*Tsutsumi et al.*, 2004] yielded two-month average Angstrom exponents of 0.99 and 0.94, which is consistent with the α values measured at the AERONET sites in Korea and Japan during spring months (Figure 2b.). Additionally, *Aoki and Fujiyoshi* [2003] show March through May mean Angstrom exponents ranging from 0.99 to 1.09 for four sites in Japan (three on Honshu and one on Hokkaido Island), from multiyear sky radiometer measurements. Therefore the data suggest that the anthropogenic fine mode pollution generated in the population centers in eastern Asia tend to more strongly influence the optical depth even in spring months when large desert dust events occur, since the dust mixes with pollution as it moves eastward and since there are more pollution events than dust events.

[17] Extremely large day-to-day variability in daily mean τ_{a500} and α at Beijing was observed in all seasons (Figures 3a and 3b). Large day-to-day variation of this magnitude is driven by a combination of many meteorological factors including air parcel trajectory, level of stagnation, temperature inversions, and dust storms associated with high winds. Very high optical depths (>1.0) occur during any time of the year, differing from most other AERONET sites that experience high τ_a but which exhibit a particular season with high τ_{a500} occurrences (e.g., biomass burning regions of Brazil and southern Africa; pollution in the mid-Atlantic United States [*Holben et al.*, 2001]). Large daily variations in Angstrom exponent also suggest significant daily variations in particle size distributions

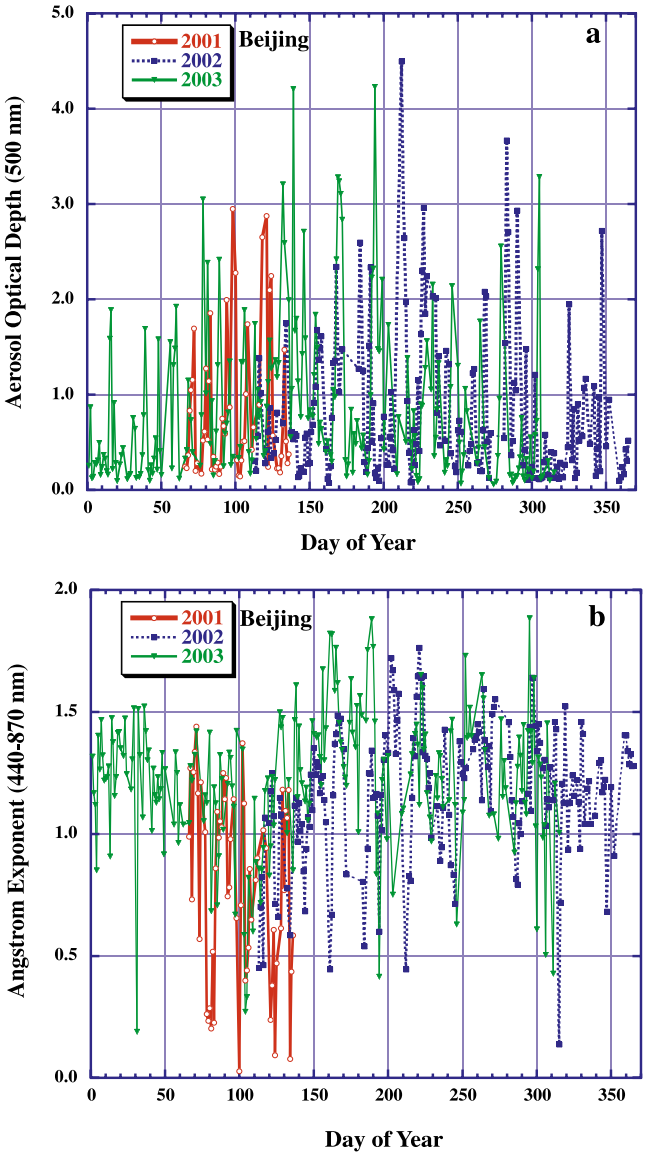

Figure 3. (a) Daily average values of τ_{a500} at Beijing, China, for portions of three years, 2001–2003, showing extremely large day-to-day variability. (b) Daily average Angstrom wavelength exponents ($\alpha_{440-870}$) for the same data as shown in Figure 3a.

ranging from almost pure coarse mode dust events ($\alpha < 0.3$) to fine mode dominated events ($\alpha > 1.1$) and many days of mixed aerosol size and type. The months of March through May in 2001 showed many days with low α that resulted from a strong influence of coarse mode desert dust aerosol.

[18] From March 20 through April 17, 2001, two AERONET Sun/sky radiometer sites were operated in the Beijing region. The permanent Beijing AERONET site is located in the center of the city, while the temporary XiangHe site was located ~80 km distant to the east-southeast in a rural area. Figures 4a and 4b show the very high correlation (r) and relatively small root mean square (rms) differences between both the daily average τ_{a500} (r = 0.99; rms = 0.10) and α (r = 0.97; rms = 0.09) at these sites during this time period. The mean τ_{a500} over this 29-day interval was 0.72 at Beijing and 0.69 at XiangHe, while the mean α was 0.79 at Beijing and 0.78 at XiangHe. This suggests that the τ_{a500} measured at the Beijing AERONET site in spring is representative of more than just the city itself but also of the area at least ~100 km in the predominant downwind direction of the city. However, this spatial relationship may differ for other seasons of the year.

[19] More than two years of instantaneous measurements (8828 observations) of $\alpha_{440-870}$ for the Amnyon, South Korea site are shown in Figure 5 as a function of τ_{a500}. A very wide range of α, from ~0.3 to ~2.0, was measured for low τ_{a500} (<0.2), suggesting a range of aerosol types from pure fine mode particles to predominantly coarse mode desert dust. A clear trend in the upper limit of α is evident, however, with maximum α decreasing steadily as τ_{a500} increases, for example all $\alpha_{440-870}$ are <1.3 for τ_{a500} > 1.5. Two factors are responsible for this trend in α with

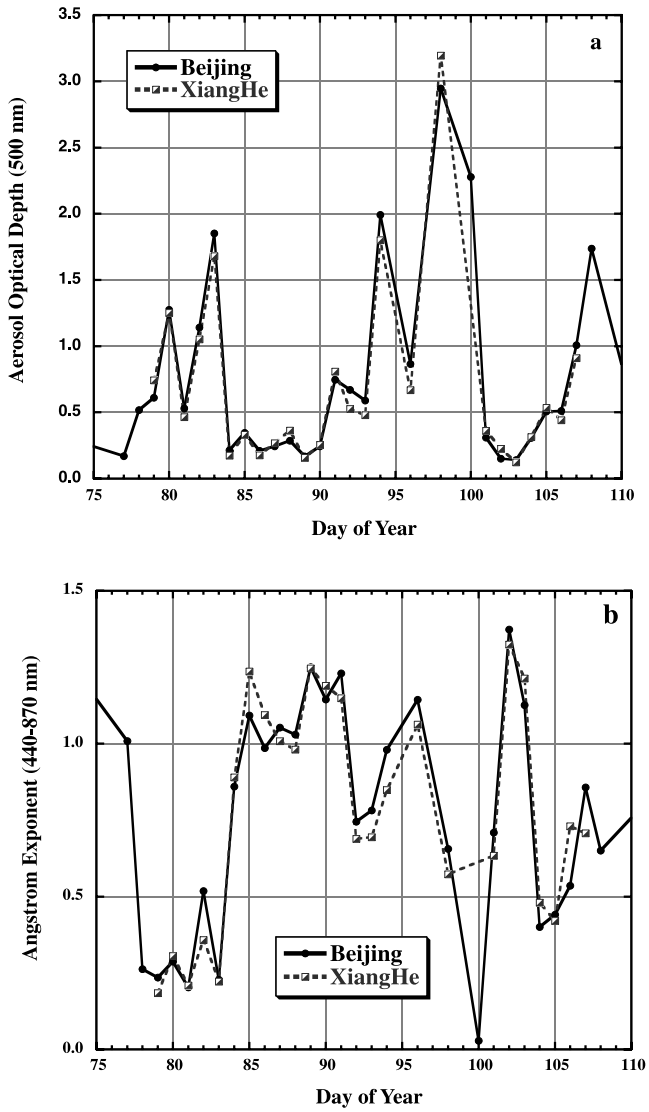

Figure 4. (a) Daily average values of τ_{a500} at Beijing and at XiangHe (~80 km to the east-southeast of Beijing) for 29 days in March–April 2001. (b) Daily average Angstrom wavelength exponents ($\alpha_{440-870}$) for the same data as shown in Figure 4a.

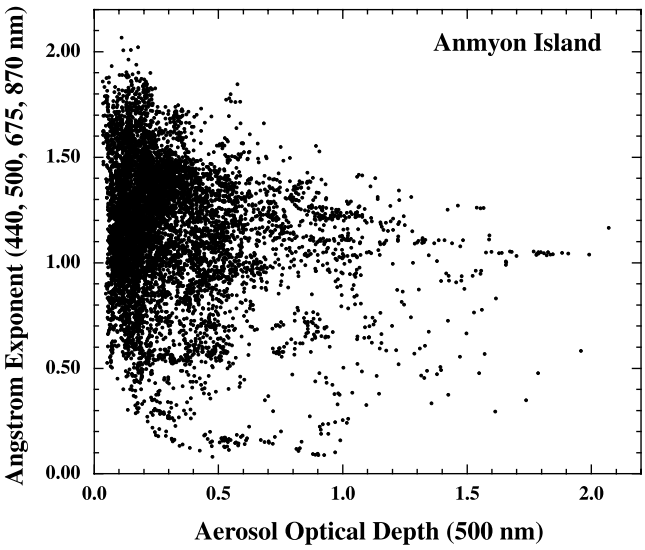

Figure 5. Instantaneous values of $\alpha_{440-870}$ versus aerosol optical depth at 500 nm at the Anmyon Island, South Korea, site for October 1999 through March 2002 (8828 individual observations shown).

increasing τ_{a500}. The first factor is that for some cases there are mixtures of both fine and coarse mode optical depths (from pollution and dust) resulting in decreasing α as the dust contribution increases. However, more importantly, an increase in fine mode particle radius as τ_{a500} increases results from particle growth due to coagulation and also from hygroscopic swelling of particle size. Coagulation rates increase as particle concentration increases [*Reid et al.*, 1998]; therefore this particle growth mechanism will be greatest at the highest τ_{a500}. Hygroscopic growth at high relative humidity (this is a coastal site downwind of the Yellow Sea) will also tend to increase τ_a as accumulation mode particles increase in size. This shift in particle size is discussed in detail for the Anmyon site from analysis of almucantar retrievals in section 3.2. Simiarly, relatively low α values (<1.2) at high τ_a have been observed for accumulation mode dominated biomass burning aerosol cases for aged smoke [*Eck et al.*, 2003a].

[20] In order to characterize the departure from linearity of the ln τ_a versus ln λ relationship (Angstrom exponent), we utilize the parameter α' defined by *Eck et al.* [1999] as the derivative of α with respect to ln λ. The parameter α' is a measure of the rate of change of the Angstrom exponent with the logarithm of wavelength. Figure 6 shows the instantaneous values of α' over more than 2 years at Anmyon, South Korea, for the same observations shown in Figure 5. When α' is equal to zero there is no curvature in the ln τ_a versus ln λ relationship and therefore the Angstrom expression fits the data best. Coarse mode dominated desert dust cases typically show α' values near zero or slightly negative [*Eck et al.*, 1999; *O'Neill et al.*, 2001]. Negative α' results when the UV to midvisible α (380 to 500 nm) is larger than the visible to near-infrared α. This occurs as a result of bimodal size distributions at relatively low optical depths with fine mode particles dominating the wavelength dependence of τ_a at short wavelengths and coarse mode particles dominating the wavelength dependence at longer wavelengths [*O'Neill et al.*, 2001]. Positive α' values typically occur in predominately fine mode bimodal size distributions with the value of α' increasing as the fine mode increasingly dominates over the coarse and as the fine mode particles increase in size [*Eck et al.*, 1999; *Reid et al.*, 1999; *Eck et al.*, 2001].

[21] Studies have well established that both desert dust and pollution from Asia are transported over 6000 to 8000 km to the tropical mid-Pacific in spring [*Husar et al.*, 1997; *Prospero et al.*, 2003; *Perry et al.*, 1999]. In January 2001 the AERONET project established a monitoring site in one of the northernmost islands in the Hawaiian chain, Midway Atoll, in part to measure the transport of Asian aerosols to mid-Pacific (there are no Pacific Ocean islands north of Midway until the Aleutian Island chain at ~52°N). Additionally, AERONET has operated long-term monitoring sites at the southeastern end of the Hawaiian island chain at the Mauna Loa Observatory (MLO) at ~3400 m altitude and near sea level on the island of Lanai. Although MLO and Lanai are ~200 km apart, this distance is small relative to the ~8000 km distance to the Asian continent, and therefore we analyze the difference in AOD of these two sites as being dominated by the difference in site altitude of ~3.4 km. Multiyear monthly means of τ_{a500} for the years 1997–2003 for months when data were available at both sites is shown in Figure 7. The resultant averages are computed from 3 to 6 years of data per month, since data were missing for some months of some years at Lanai. The obvious seasonal trend is a distinct increase in τ_{a500} in March through May at both sites. The months of July through January exhibit relatively little variability of τ_{a500}. It is noted that since MLO is the AERONET calibration site, the reference instrument data there is of high accuracy, ~0.003 at 500 nm, while at Lanai (an AERONET field site instrument) the accuracy is ~0.015 [*Eck et al.*, 1999; *Schmid et al.*, 1999]. For the Mauna Loa Observatory data,

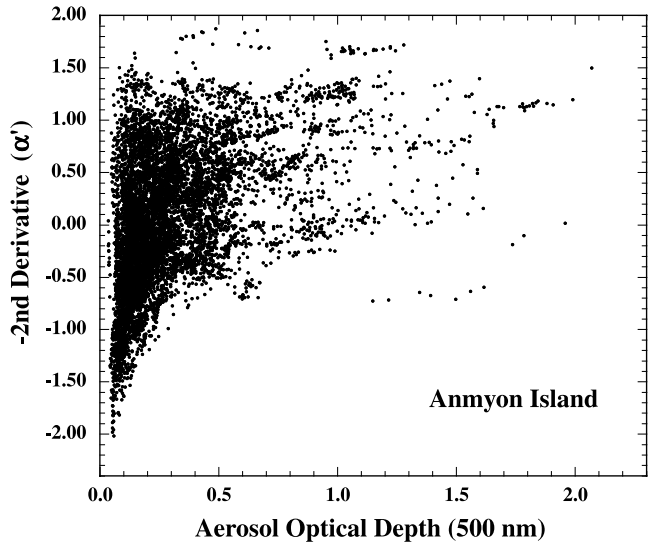

Figure 6. Values of α' (dα/d lnλ) computed from instantaneous τ_a values at 380, 500, and 870 nm at Anmyon Island, South Korea, as a function of aerosol optical depth at 500 nm, for the same observation times as the data in Figure 5 (October 1999 through March 2002).

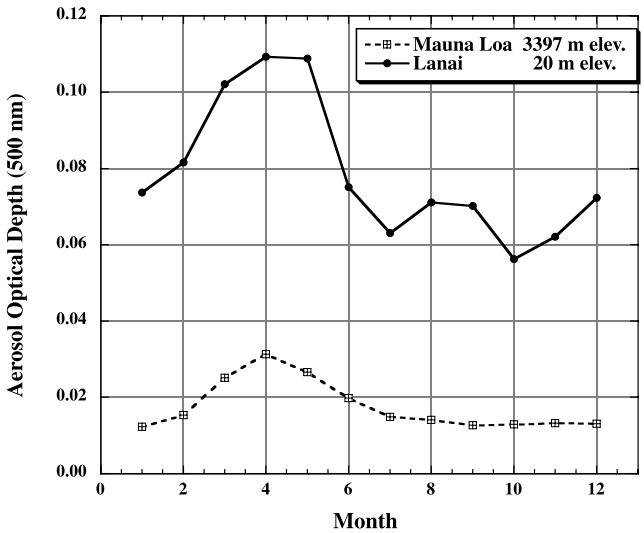

Figure 7. Monthly means of τ_{a500} for the Lanai and Mauna Loa Observatory sites (both in Hawaii, ~200 km apart). Means were computed only from months where both sites had measurements, resulting in a range of 3–6 years of data averaged for each month, from the 1997–2003 time interval. For the Mauna Loa Observatory site only data from air mass 2 to 5 in the morning (when there typically is descending flow) were utilized to compute daily means in order to attempt to characterize the τ_{a500} of the upper tropospheric plus stratospheric aerosol only. For the Lanai site, data from the compete diurnal cycle were utilized to compute daily means.

we average only the morning data from air mass 2 through 5 (<1.5 hour time interval) to obtain an estimate of the upper tropospheric plus stratospheric aerosol only. Downslope flow occurs during this time interval, as opposed to upslope flow and convection from midmorning through the afternoon that can bring marine boundary layer aerosols above the station altitude [*Dutton et al.*, 1994]. The stratospheric volcanic aerosol contribution to τ_a from the Mount Pinatubo eruption in June 1991 is insignificant after 1995 [*Barnes and Hoffman*, 1997], hence the data shown here for MLO for July through January may be considered as representative values of upper tropospheric plus stratospheric background τ_{a500} in the tropical mid-Pacific (average of ~0.013). For the nonspring months of July–January at Lanai the average total column τ_{a500} (~0.067, for these years) can be considered to be dominated by sea salt [*Smirnov et al.*, 2003], with τ_{a500} below 3.4 km at Lanai ~0.054, being the truly maritime component of the total column optical depth. Therefore, for the months of July–January, ~20% of the total column tropical mid-Pacific aerosol optical depth is above 3.4 km altitude.

[22] *Liu et al.* [2003] analyzed the outflow of Asian pollution over the Pacific Ocean and found maximum carbon monoxide outflow in March–April due to frontal lifting ahead of cold fronts in China and additionally due to deep convection over biomass burning regions of Southeast Asia during the peak burning months. As noted previously, these spring months are also the season of maximum desert dust event frequency in Asia (see Figure 2b). From Figure 7 it is seen that the three month March through May mean τ_{a500} at Lanai is ~0.040 higher than the July through January mean, while at MLO the March–May mean is ~0.014 higher than the July–January mean. Therefore ~35% of the total column enhancement in spring is due to aerosol above 3.4 km altitude in the mid-Pacific at ~20°N.

[23] Monthly means of τ_{a500} for the three Hawaiian island sites, including Midway, in 2001 are shown in Figure 8. In this year the spring peak in τ_{a500} is also obvious but is of somewhat longer duration at MLO than the long-term mean (Figure 7), with the highest monthly means occurring between February and June. Similar to MLO, the τ_{a500} at Lanai in 2001 also shows a broader spring peak than for the multiyear average. The spring enhancement near sea level at Midway is much greater than that observed at Lanai primarily due to Midway being located ~7.5° farther north in latitude and also ~2000 km closer to Asia. The April monthly mean τ_{a500} at Midway was 0.21 in 2001 with daily average values as high as 0.41 ($\alpha_{440-870}$ was 0.45 on this peak day, April 24, 2001). High τ_{a500} days in April 2001 at Midway were associated with transport trajectories from dust regions in northern China and Mongolia as determined by the Hybrid Single Particle Lagrangian Integrated Trajectory (HYSPLIT) model (http://www.arl.noaa..gov/ready/hysplit). *Liu et al.* [2003] show that zonal transport from Asia to mid-Pacific strengthens as latitude increases from ~20°N to ~30°N in the spring months. Surface air sampling measurements at Midway of components of both anthropogenic pollution and soil dust aerosols by *Prospero et al.* [2003] also show a marked maximum in spring, from long-term monitoring over a 20-year interval. Monthly average wind speeds at both Lanai and Midway in 2001 show no seasonal trend (average speed in spring differs by less than 1 m/sec compared to nonspring months) therefore

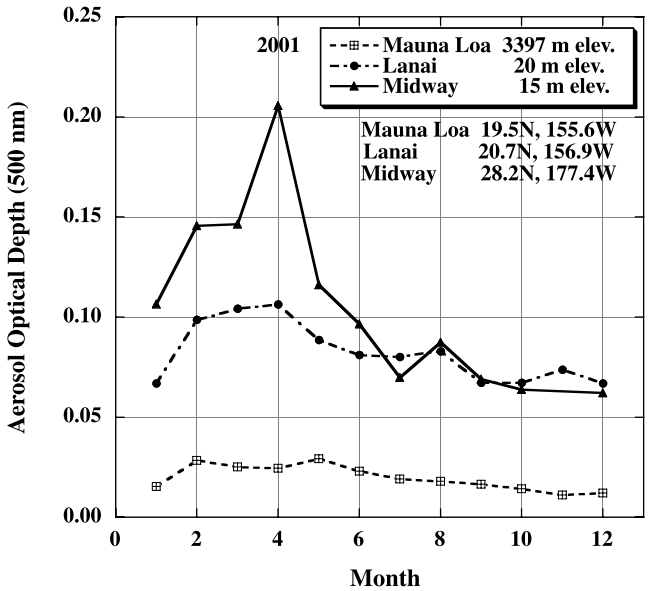

Figure 8. Monthly means of τ_{a500} for the Midway, Lanai, and Mauna Loa Observatory sites in 2001 (all in the Hawaiian Island chain). For the Mauna Loa Observatory site only data from air mass 2 to 5 in the morning were utilized to compute daily means, while for the other two sites data from the entire diurnal cycle were utilized.

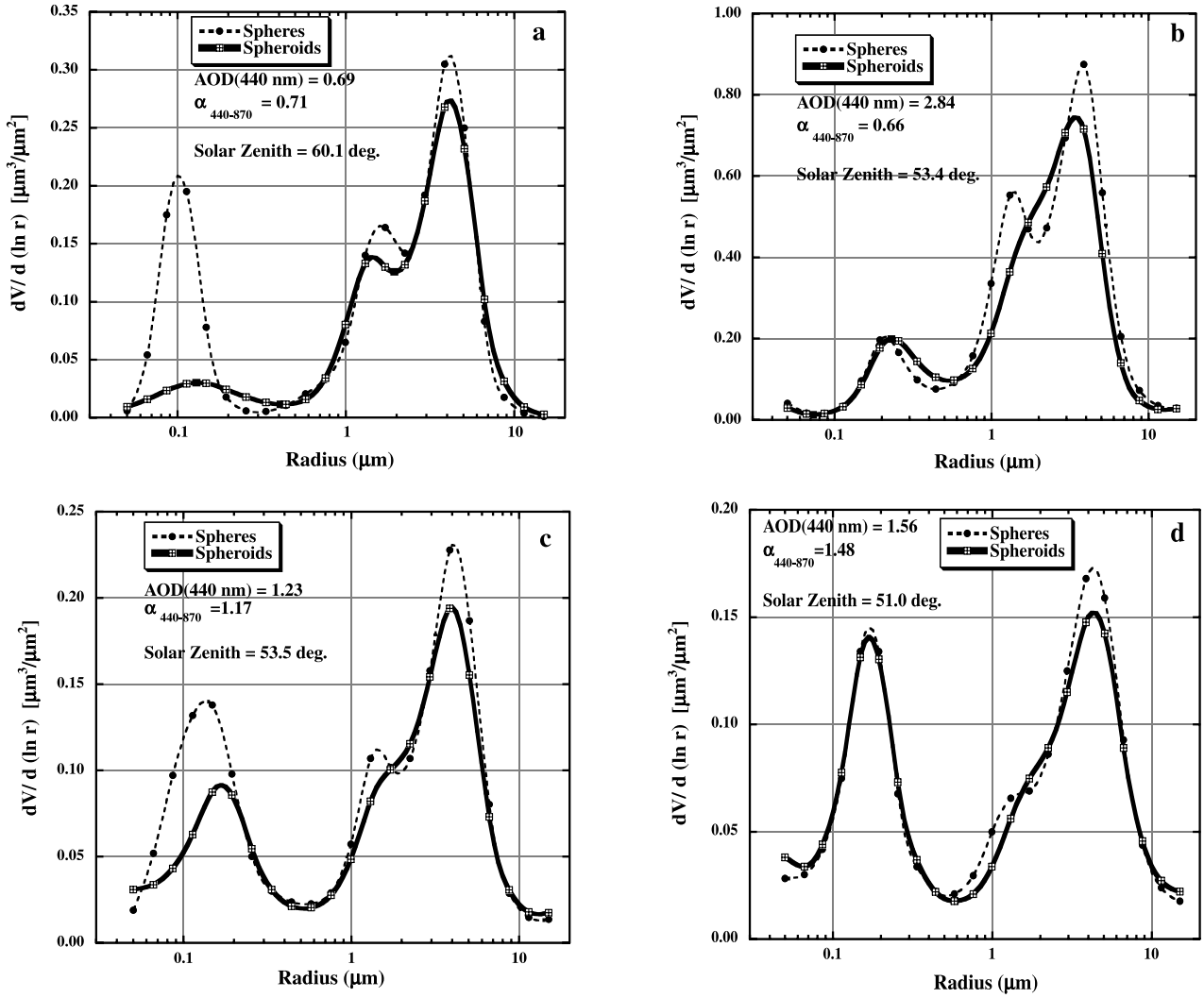

Figure 9. Comparisons of aerosol size distribution retrievals resulting from two different assumptions of particle shape, spherical particle shape versus spheroid particle shape (with a fixed aspect ratio distribution). Four cases are shown from Beijing data: (a) on April 16, 2001, with moderate τ_a and low $\alpha_{440-870}$, (b) on April 8, 2001, with very high τ_a and low $\alpha_{440-870}$, (c) on June 3, 2002, with high τ_a and moderate $\alpha_{440-870}$, and (d) on March 12, 2001, with high τ_a and high $\alpha_{440-870}$.

the observed enhanced sea salt τ_{a500} associated with higher wind speeds at Midway [*Smirnov et al.*, 2003] does not contribute to the higher spring τ_{a500} measured at these sites. Both GOCART model and MODIS satellite measurements of monthly mean τ_a at Midway in April 2001 showed differences of ~0.06 with AERONET measurements [*Chin et al.*, 2004], with GOCART lower and MODIS higher than AERONET. Monthly mean AERONET τ_{a500} at both Midway and Lanai are nearly equal ($\Delta\tau_{a500} < 0.01$) from July through December (Figure 8) suggesting that a large area of the tropical to subtropical mid-Pacific has relatively homogeneous τ_a in the nonspring months when Asian aerosol transport does not affect the region.

3.2. Aerosol Size Distributions

[24] Due to the pervasive presence of complex aerosol mixtures in central Asia, there are often various combinations of both dominantly spherical shape particles (pollution) and distinctly nonspherical particles characteristic of airborne soil dust. Since the particle size distributions retrieved by AERONET are largely determined by the angular distribution of sky radiances (and additionally from τ_a spectra), the scattering characteristics of nonspherical particles need to be accounted for in the size distribution retrievals. The particle shape assumption that we utilize in the retrievals presented in this study is spheroid with a fixed aspect ratio distribution [*Dubovik et al.*, 2002b]. Although this assumption is a simplification of the actual particle shapes of desert dust (scanning electron micrographs show complex shapes [*Reid et al.*, 2003]) the spheroid particle assumption accounts for most of the observed features of nonspherical dust scattering [*Dubovik et al.*, 2002a, 2002b].

[25] Examples of size distribution retrievals from the *Dubovik and King* [2000] algorithm comparing the influence of assumed particle shape (spherical and spheroid) are shown in Figure 9. These are retrievals made from Cimel Sun/sky radiometer data acquired at the Beijing site for various types of aerosol mixtures (fine versus coarse mode

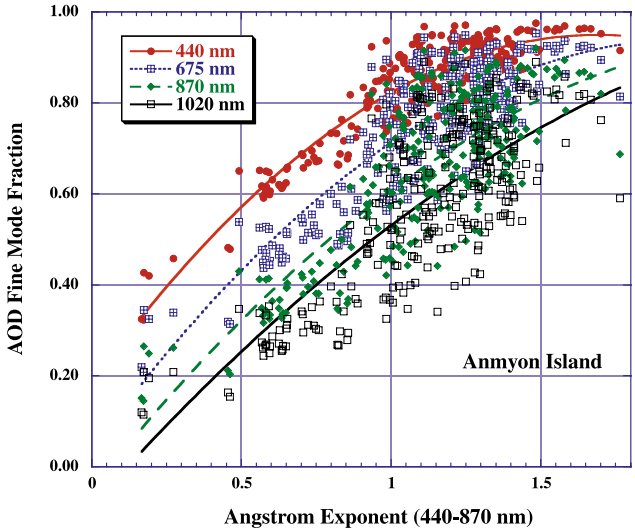

Figure 10. The fine mode fraction of aerosol optical depth at four wavelengths as a function of Angstrom exponent ($\alpha_{440-870}$) at Anmyon Island, South Korea, for October 1999 through March 2002, for almucantar retrievals when $\tau_{a440} > 0.40$.

relative contributions). In Figure 9a are shown retrievals from April 16, 2001, where coarse mode aerosol is dominant, $\alpha_{440-870} = 0.71$ and $\tau_{a440} = 0.69$. For this type of coarse mode (and nonspherical) dominated case the assumption of spherical particles yields a false fine mode peak of very small particles [*Dubovik et al.*, 2000, 2002a, 2002b], and additionally a large wavelength dependence of the real refractive index (not shown). The false fine mode results from the phase function in the middle scattering angle range (70°–150°) being greater for spheroids than for spheres, thus forcing the occurrence of false fine mode particles when spherical shape is assumed [*Dubovik et al.*, 2000]. The assumption of spheroid shaped particles essentially eliminates the false fine mode, yet retains a fine mode component of somewhat larger particle size, consistent with the Angstrom exponent of 0.71. Figure 9b shows a case from April 8, 2001, with similar Angstrom exponent ($\alpha_{440-870} = 0.66$) but with much higher aerosol loading, $\tau_{a440} = 2.84$. Here we see that the spherical particle assumption did not result in a false fine mode peak of very small particles, in this case since multiple scattering in the optically thick aerosol layer minimized the nonspherical scattering effects. The spheroid shape assumption did however result in reduced bimodality of the coarse mode relative to the spherical particle assumption. A case with significantly more fine mode aerosol present is shown in Figure 9c where $\alpha_{440-870} = 1.17$ and $\tau_{a440} = 1.23$. Here the main difference between the spherical and spheroid shape assumption retrievals is the shift in fine mode particle size to larger sizes in the spheroid retrieval due to the influence of a false fine mode anomaly in the spherical assumption retrieval resulting from the nonspherical scattering effects of the coarse mode particles (similar to Figure 9a). In Figure 9d we show the comparison of retrievals for a strongly dominated fine mode aerosol case, $\alpha_{440-870} = 1.48$ and $\tau_{a440} = 1.56$. Here there is little difference in the retrievals, especially for the fine mode particles. This demonstrates that there is relatively little sensitivity to particle shape in the retrievals for fine mode particle scattering [*Dubovik et al.*, 2002a, 2002b]. Therefore we utilize the spheroid particle assumption retrievals for all cases since artifacts from nonspherical coarse particle scattering are minimized and the integrity of the fine mode retrievals is maintained.

[26] In our investigation of the retrievals of aerosol size distributions, we have chosen to separate observations that are dominated by coarse mode aerosols (desert dust) from those dominated by fine mode particles (predominately pollution, but sometimes also biomass burning aerosols). We have analyzed the relationship between Angstrom exponent and τ_a fine mode fraction ($\tau_{aFine}/\tau_{aTotal}$) in order to stratify the data. Fine and coarse mode optical depths were computed from the retrieved size distributions and refractive indices, with particles of volume radius <0.6 μm being identified as fine mode and with radius >0.6 μm as being coarse mode particles.

[27] The relationship between fine mode fraction of optical depth and $\alpha_{440-870}$ for more than 2 years of observations at Anmyon Island, South Korea is shown in Figure 10. Fine mode fraction of τ_a at a fixed α value varies strongly as a function of wavelength since fine mode particles (peak radius ranging from ~0.12 to 0.30 μm) scatter light most effectively at wavelengths similar to particle size, and are much less effective light scatters when wavelength is significantly longer than particle size. We have selected as a threshold $\alpha_{440-870} = 0.75$ to separate fine versus coarse mode dominated aerosol cases since fine mode fraction at 675 nm is ~50% at this value. The 675 nm wavelength was chosen since it is nearly in the center of the total downwelling shortwave solar spectrum, with ~50% of the energy falling either above or below this wavelength. As Angstrom exponent increases, especially >0.9, there is much greater scatter in the fine mode fraction for a given $\alpha_{440-870}$ value. This is largely the result of differences in fine mode particle size and the reduction in α magnitude as fine mode particles grow from aging and/or hygroscopic growth [*Reid et al.*, 1999; *Eck et al.*, 2001, 2003a].

[28] Aerosol size distribution retrievals for cases with $\tau_{a440} > 0.4$ that are predominantly fine mode ($\alpha_{440-870} > 0.75$) at Anmyon Island for more than two years of data are shown in Figure 11. The data were further stratified by the magnitude of aerosol optical depth with an average of 30 individual almucantar scan retrievals averaged for each of eight τ_{a440} bins, ranging from 0.41 to 1.32. The average $\alpha_{440-870}$ for each of these eight bins averaged from 1.11 to 1.25, thus implying an average fine mode fraction at 675 nm ranging from ~70 to 80% (Figure 10). Fine mode particle size was observed to steadily increase as τ_a increased in both the modal maximum value and expansion of the fine mode boundary towards larger radius while the boundary on the small particle side of the fine mode was relatively constant. The peak modal volume radius of the highest fine mode optical depth cases observed (mean $\tau_{a440} = 1.32$) was ~0.25 μm with $\alpha_{440-870} = 1.11$, and fine mode fraction of τ_a at 675 nm of ~90%. These are very large fine mode particles, similar in size to pollution aerosol for the U.S. mid-Atlantic region at high optical depth [*Dubovik et al.*, 2002a] and for aged smoke transported from peat fires in Russia [*Eck et al.*, 2003a]. As previously mentioned in

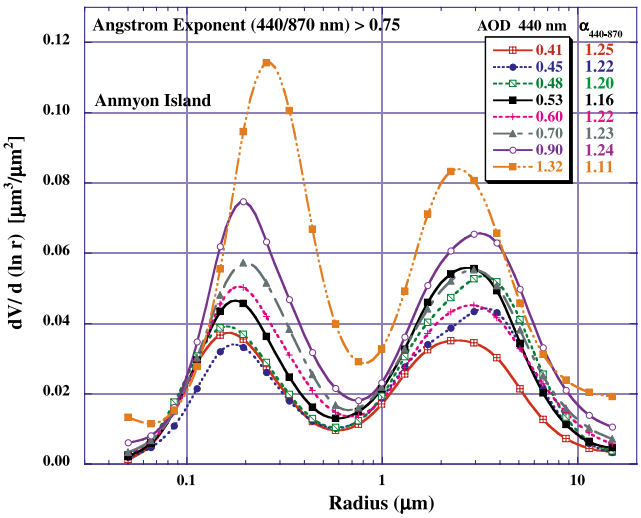

Figure 11. Aerosol volume size distributions at Anmyon Island, South Korea, for predominately fine mode aerosol optical depth cases ($\alpha_{440-870}$ > 0.75), with τ_{a440} varying from 0.41 to 1.32. Each size distribution is an average computed from 30 individual almucantar scan retrievals.

relation to analysis of the Angstrom exponent (Figure 5), this tendency towards larger size fine mode particles at higher τ_a is likely due to increasing rates of coagulation as τ_a (and therefore concentration) increases [*Reid et al.*, 1998], and also due to hygroscopic growth at higher RH as a result of the presence of certain aerosol species such as sulfates, which are produced in coal combustion. For the coarse mode, there is no systematic trend in particle size as a function of τ_a, and mean maximum radius of the volume distribution is ~2.5 µm.

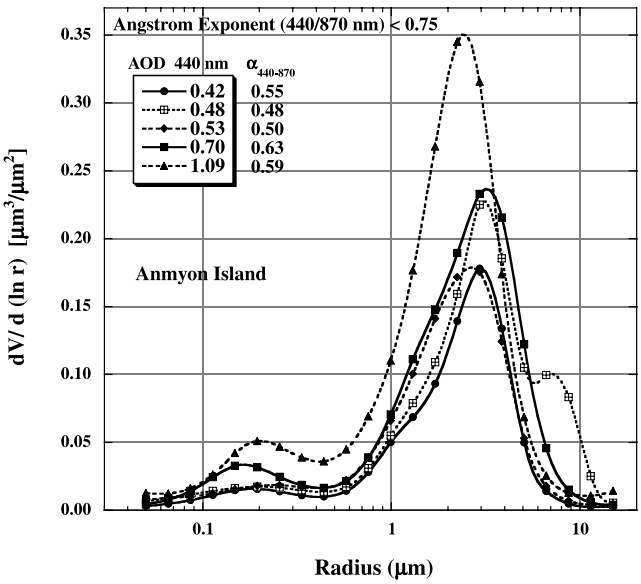

Figure 12. Aerosol volume size distributions at Anmyon Island, South Korea, for predominately coarse mode aerosol optical depth cases ($\alpha_{440-870}$ < 0.75), with τ_{a440} varying from 0.42 to 1.09. Each size distribution is an average computed from 7 individual almucantar scan retrievals.

[29] The size distributions for the coarse mode desert dust dominated cases ($\alpha_{440-870}$ < 0.75) for Anmyon Island are shown in Figure 12. Many fewer cases occurred at low $\alpha_{440-870}$ (see Figure 10) resulting in each of the five τ_a bins containing an average of only 7 individual almucantar scan retrievals. The mean $\alpha_{440-870}$ for each of the five bins ranged from 0.48 to 0.63. The volume median radius of the coarse mode ranged from ~2.1 to 2.9 µm with geometric standard deviation of ~1.75 to 1.80 with no trend in either as a function of τ_a. This compares to coarse mode parameters from other desert dust source regions in the Sahara and Saudi Arabia (also from AERONET retrievals) of volume median radius ranging from ~1.9 to 2.5 µm with geometric standard deviation of ~1.70 to 1.84 [*Dubovik et al.*, 2002a]. Comparisons of coarse mode desert dust size distribution retrievals from several in situ measurement techniques were compared to retrievals from the *Dubovik and King* [2000] algorithm for long-range transported Saharan dust [*Reid et al.*, 2003]. *Reid et al.* [2003] found a very large range in volume median radius (radius varied from 1.25 to 4.5 µm) from the various in situ measurement techniques (due to various systematic biases for different techniques), with AERONET retrieved size distributions showing an intermediate value in coarse mode particle size (radius ~2.0 µm).

[30] Aerosol size distributions of the predominantly fine mode τ_a cases ($\alpha_{440-870}$ > 0.75) for Beijing, China are shown in Figure 13. As was also the case for Anmyon, the size distribution in each of eight optical depth size bins is an average of retrievals made from 31 individual almucanatar scans. Also similar to Anmyon, the fine mode distributions at Beijing showed a shift to larger size particles as the aerosol optical depth increased. The fine mode particle size at high τ_a at Beijing is not quite as large as at Anmyon (especially at equal τ_a levels). For example, at τ_{a440} = 0.68–0.70 the peak fine modal radius at Beijing is ~0.17 µm while at Anmyon it is ~0.20 µm, with a broader geometric standard deviation at Beijing (1.70) than at Anmyon (1.61).

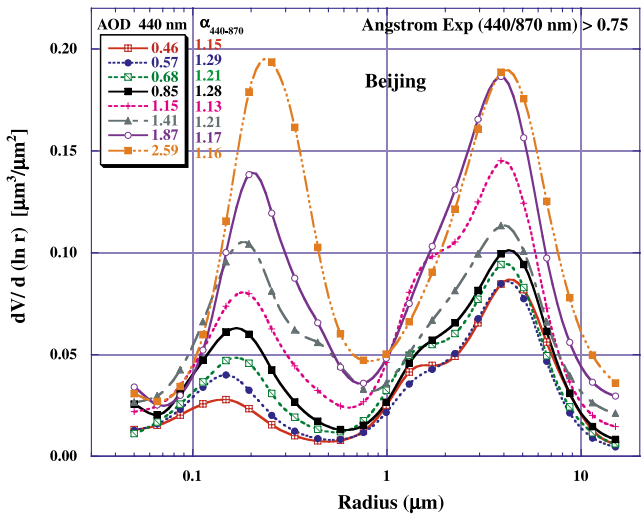

Figure 13. Aerosol volume size distributions at Beijing, China, for predominately fine mode aerosol optical depth cases ($\alpha_{440-870}$ > 0.75), with τ_{a440} varying from 0.46 to 2.59. Each size distribution is an average computed from 31 individual almucantar scan retrievals.

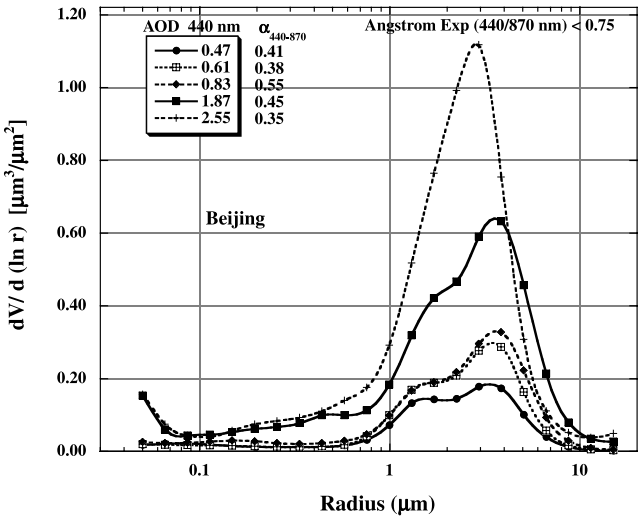

Figure 14. Aerosol volume size distributions at Beijing, China, for predominately coarse mode aerosol optical depth cases ($\alpha_{440-870} < 0.75$), with τ_{a440} varying from 0.47 to 2.55. Each size distribution is an average computed from 8 individual almucantar scan retrievals.

This difference may possibly be the result of large daily production of fresh (and therefore smaller) accumulation mode particles in the city of Beijing and also possibly from differences in particle growth through coagulation in some cases of aerosol transport from China to the Anmyon Island site. Additionally, hygroscopic particle growth may be greater at Anmyon when aerosol is transported over the Yellow Sea to the site, thus resulting in higher relative humidity and also possibly adding some strongly hygroscopic sea salt to the aerosol mixture. The coarse particle mode at Beijing associated with the predominantly fine mode τ_a cases (Figure 13) shows little dynamic change as a function of τ_a (similar to Anmyon) but with a suggestion of some bimodality within the coarse mode that was not present at Anmyon. The coarse mode τ_a dominated cases ($\alpha_{440-870} < 0.75$) of desert dust aerosol for Beijing shown in Figure 14, are computed from a far fewer number of almucantar scans (8 per τ_a bin) than the fine mode, due to dust dominated cases being present mainly in the spring while fine mode dominated cases are present year round. Similar to the coarse mode associated with the fine mode dominated cases in Beijing, the desert dust coarse mode cases exhibit bimodality not present in the Amnyon retrievals for dust cases. The reasons for these differences in the coarse mode size distributions between these two sites are unknown.

3.3. Single Scattering Albedo

[31] Single scattering albedo retrievals assuming spherical or spheroid particle shape are compared for four case studies at differing Angstrom exponent and τ_a levels in Figure 15. The spectral variation of aerosol single scattering albedo for these four specific cases in Beijing correspond to the size distribution retrievals from the same almucantar scans presented in Figure 9. As seen in Figure 15, the retrieval of ω_0 varies little (typically < 0.01) as a result of the two different particle shape assumptions, consistent with the expected influence of particle shape on ω_0 retrieval [*Mishchenko et al.*, 1997; *Dubovik et al.*, 2002b]. The decrease in slope of ω_0 with wavelength as Angstrom exponent decreases (increasing coarse mode fraction) is consistent with the changes in spectral ω_0 observed at Bahrain in the Persian Gulf [*Smirnov et al.*, 2002] as a result of the variation in relative influence of fine mode pollution versus coarse mode desert dust. Spectral dependence of ω_0 in fine mode dominated aerosol (high Angstrom exponent) exhibits decreasing ω_0 as wavelength increases partly due to the relatively constant imaginary index of refraction of black carbon (the principal absorbing component in the fine mode) as a function of wavelength [*Bergstrom et al.*, 2002; *Eck et al.*, 2003b].

[32] The spectral ω_0 of the predominately fine mode τ_a cases ($\alpha_{440-870} > 0.75$) for the Anmyon Island site, for the same data corresponding to the size distribution retrievals in Figure 11, are shown in Figure 16. There was no trend in ω_0 as a function of τ_a observed in the data and relatively little variability in ω_0, ~0.02 in the visible and <0.04 in the infrared. Values of ω_0 in the midvisible (550nm; from interpolation between 440 and 675 nm data) at Anmyon ranged from ~0.92 to 0.94, which is very similar to the ω_{0550} measured in polluted air masses during ACE-Asia (spring 2001) from shipboard in situ measurements near Korea and Japan, where ω_0 was 0.94 ± 0.03 at ambient relative humidity [*Carrico et al.*, 2003]. In situ measurements from both aircraft and ship of fine mode (pollution) aerosol off the coasts of Korea and Japan during ACE-Asia showed that the pollution aerosol was moderately to strongly hygroscopic [*Anderson et al.*, 2003; *Carrico et al.*, 2003]. As mentioned previously, the increase in particle size as τ_a increased at Anmyon Island may have had a contribution

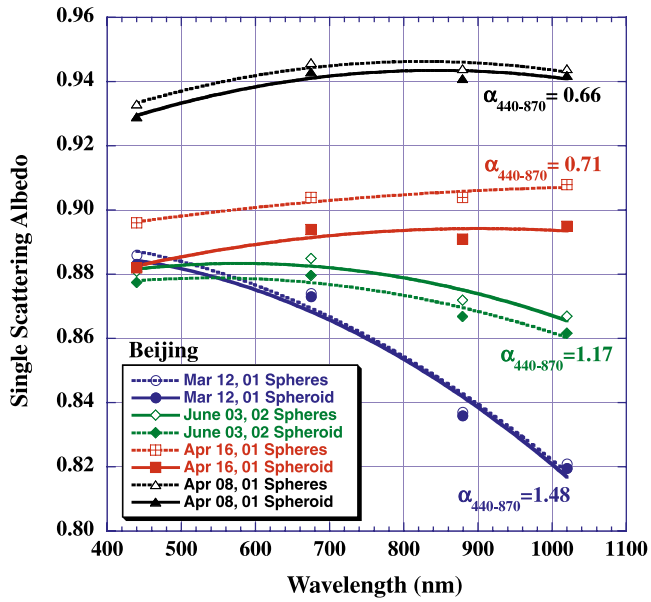

Figure 15. Comparisons of single scattering albedo retrievals resulting from two different assumptions of particle shape, spherical particle shape versus spheroid particle shape (with a fixed aspect ratio distribution). These four cases of Beijing data correspond to the same cases shown in Figure 9 for the size distributions.

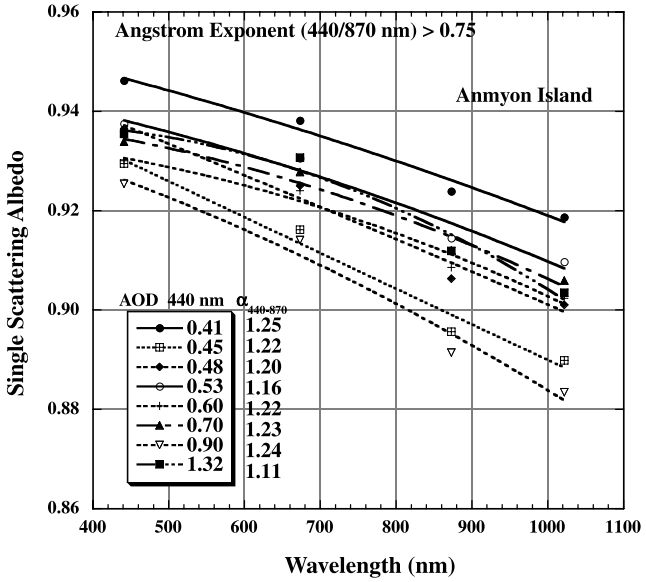

Figure 16. Aerosol single scattering albedo at Anmyon Island, South Korea, for predominately fine mode aerosol optical depth cases ($\alpha_{440-870} > 0.75$), with τ_{a440} varying from 0.41 to 1.32. Each ω_0 is an average computed from 30 individual almucantar scan retrievals. These ω_0 retrievals correspond to the same cases shown in Figure 11 for the size distributions.

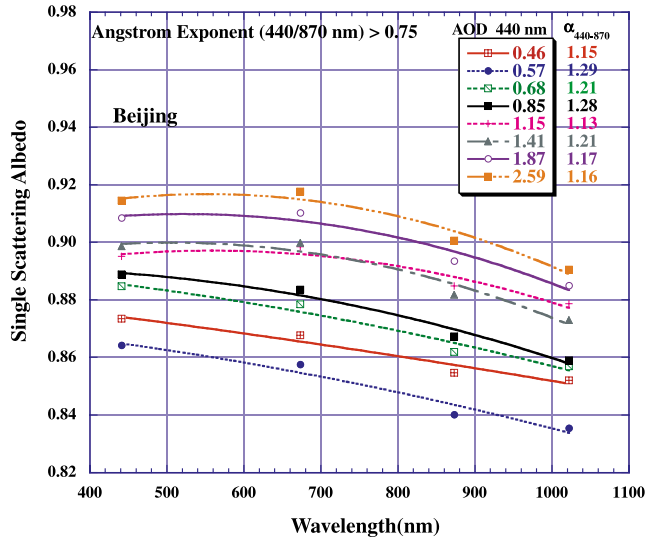

Figure 17. Aerosol single scattering albedo at Beijing, China, for predominately fine mode aerosol optical depth cases ($\alpha_{440-870} > 0.75$), with τ_{a440} varying from 0.46 to 2.59. Each ω_0 is an average computed from 31 individual almucantar scan retrievals. These ω_0 retrievals correspond to the same cases shown in Figure 13 for the size distributions.

from hygroscopic particle growth, however the lack of trend in ω_0 or imaginary refractive index as a function of τ_a, suggests that relative humidity does not strongly influence column-integrated ω_0 at this site or perhaps a combination of factors results in a lack of observed trend. In contrast, single scattering albedo measured at the surface (shipboard) in spring 2001 during ACE-Asia showed a strong correlation with surface relative humidity [*Markowicz et al.*, 2003].

[33] Single scattering albedo retrieved at Beijing, as a function of τ_a for predominately fine mode aerosol ($\alpha_{440-870} > 0.75$) from the same almucantar scans as the size distributions given in Figure 13, are shown in Figure 17. The ω_0 values at Beijing are lower than at Anmyon, especially in the visible, possibly due to the maritime influence (Yellow Sea) of sea salt aerosol and higher relative humidity at Anmyon, and also possibly due to aging of aerosols that are transported over the sea from China to Anmyon. Another possible factor in these differences is that fine mode pollution produced in Beijing may be more absorbing than pollution from sources in South Korea, due to differences in fuel types, combustion methods, and pollution control technology. A distinct trend of increasing ω_0 (at all wavelengths) as τ_{a440} increased was observed at Beijing. This results from a combination of increasing fine mode particle size as τ_a increased (Figure 13) coupled with decreasing imaginary refractive index, from ~0.016 at $\tau_{a440} \approx 0.5$ to ~0.012 at $\tau_{a440} \approx 2.5$. These trends in particle size, and imaginary refractive index are consistent with possible hygroscopic growth but also with other possible aerosol aging mechanisms such as gas-to-particle conversion, condensation, and coagulation. The magnitude of this ω_0 trend is significant with a range of ~0.05 over a range of τ_{a440} from ~0.5 to ~2.6.

[34] A comparison of spectral ω_0 for fine mode dominated cases ($\alpha_{440-870} > 0.75$) for four sites, Anmyon, Beijing, Shirahama, and Yulin is presented in Figure 18. Shown are average ω_0 computed for all almucanatr scans when $\tau_{a440} > 0.40$. The two continental Chinese sites of Yulin and Beijing show similar ω_0 values, within ~0.01 at most wavelengths.

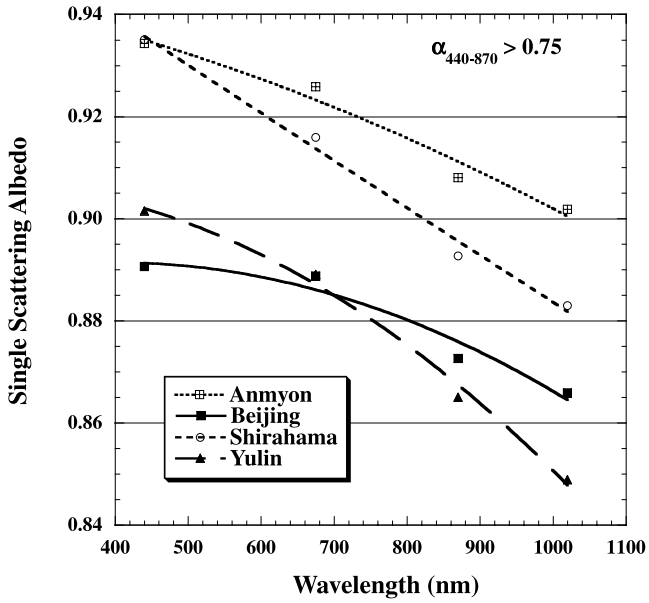

Figure 18. Comparison of aerosol single scattering albedo at four sites (Anmyon, Beijing, Shirahama, and Yulin) for predominately fine mode aerosol optical depth cases ($\alpha_{440-870} > 0.75$). The mean of all cases where $\tau_{a440} > 0.40$ at each site are shown.

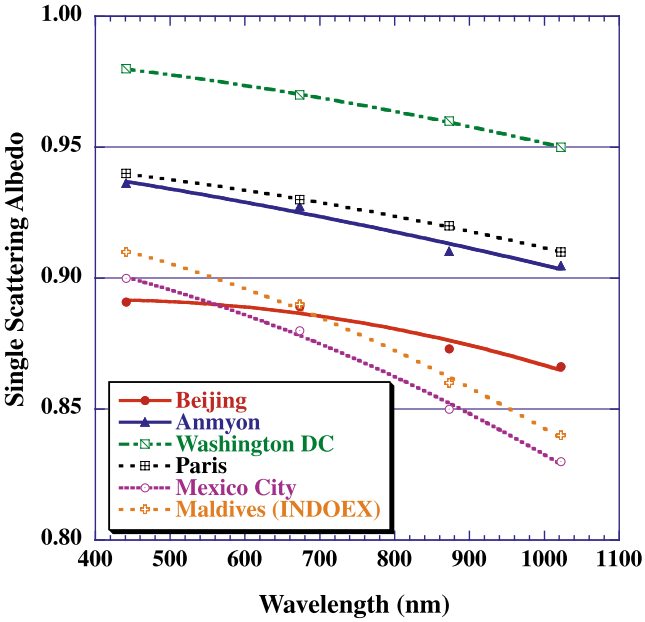

Figure 19. Comparison of aerosol single scattering albedo at urban/industrial pollution sites in the AERONET network. The data for Beijing and Anmyon are for cases where $\alpha_{440-870} > 0.75$, in order to characterize pollution aerosol. The mean of all cases where $\tau_{a440} > 0.40$ at each site are shown. The data for Washington, D. C. (GSFC), Paris (Creteil), and Mexico City are from Table 1 in *Dubovik et al.* [2002a].

The two coastal sites (Anmyon and Shirahama) further east in South Korea and Japan show similar values to each other with $\Delta\omega_0$ ranging from near zero to ~0.02 at the 4 wavelengths, while exhibiting ω_0 that is ~0.03 to ~0.04 higher than the two Chinese continental sites. In addition to the factors discussed in the previous paragraph for differences between Beijing and Anmyon pollution aerosol (relative humidity, sea salt at coastal sites, aerosol aging during transport, and fuel combustion differences) it is also noted that both Chinese sites are urban centers with Beijing a mega-city of ~14 million and Yulin a major Chinese coal production center. In contrast the coastal sites of Shirahama, Japan and Anmyon, Island, South Korea are relatively rural with much lower local population density and less local industry.

[35] The spectral single scattering albedo of Beijing and Anmyon for fine mode dominated cases are compared to values retrieved at AERONET sites located in other global urban centers, and also regions affected by transport of pollution primarily from fossil fuel combustion (Maldives), in Figure 19. The ω_0 data for the sites in Mexico City, Paris (Creteil site, a suburb), Washington, D. C. (GSFC site is located in a suburb of Washington, D. C.), and Maldives (Kaashidhoo) are from Table 1 of *Dubovik et al.* [2002a]. The data shown in Figure 19 are averages for each site from almucantar scans where $\tau_{a440} > 0.40$, and additionally for Beijing and Anmyon only for cases where $\alpha_{440-870} > 0.75$ to exclude desert dust aerosol events (the other urban/pollution sites are not subjected to dust dominated events with high τ_a). The spectral ω_0 for the urban/industrial pollution aerosol are nearly equal between Beijing, Mexico City, and Maldives at 440 and 675 nm, while divergence exists in the near infrared wavelengths, because the spectral dependence is less at Beijing than at Mexico City and Maldives. The lower spectral dependence of ω_0 at Beijing relative to the other two highly absorbing sites is due to the larger contribution of coarse mode particles at Beijing thus increasing the relative scattering contribution at longer wavelengths. As discussed in further detail in *Dubovik et al.* [2002a], the variability in aerosol absorption in urban regions results from a variety of factors including differences in fuel types, emission conditions, long-range transport or aging, and meteorological conditions. The strong absorption in the visible wavelengths in Beijing, Mexico City, and Maldives is due to relatively high concentrations of soot or black carbon in the aerosol. The relatively low absorption of the aerosol in Washington, D. C., in the summer months (the only months where $\tau_{a440} > 0.40$ events are common) is a result of lower concentrations of black carbon in combination with water-soluble aerosol at higher relative humidity that results in fine mode particle growth and an increase in light scattering coefficient [*Kotchenruther and Hobbs*, 1998]. Aerosol absorption adjacent to the Yellow Sea (Anmyon) is significantly less absorbing than over the Arabian Sea AERONET site (Maldives). Similarly, in situ aerosol absorption measurements at the surface during ACE-Asia over the Sea of Japan showed less absorption than over the Arabian Sea during the INDOEX campaign in 1999 [*Markowicz et al.*, 2003; *Ramanathan et al.*, 2001].

[36] A comparison of desert dust single scattering albedo from data collected in the spring of 2001 at Dunhuang (China), Beijing, and Anmyon is shown in Figure 20. Also

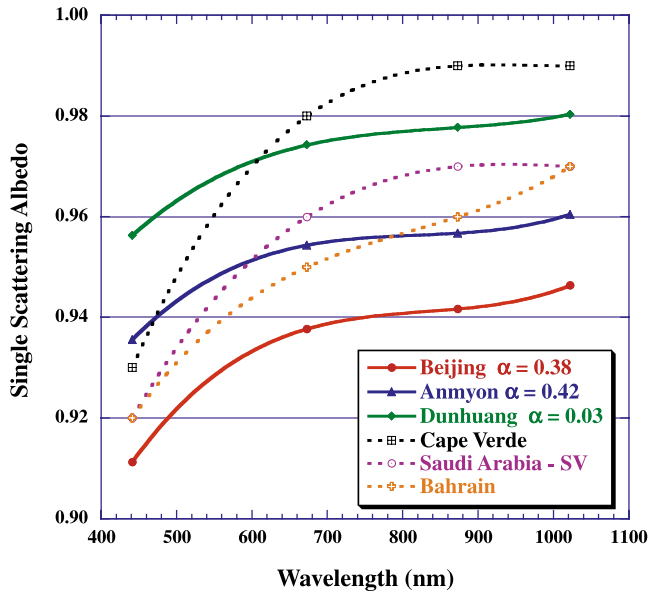

Figure 20. Comparison of aerosol single scattering albedo for dust cases ($\alpha_{440-870} < 0.75$) at three Asian sites in spring 2001: Dunhuang, Beijing, and Anmyon. Also shown are data from Table 1 in *Dubovik et al.* [2002a] for three other dust-dominated sites in the AERONET network: Bahrain, Saudi Arabia, and Cape Verde.

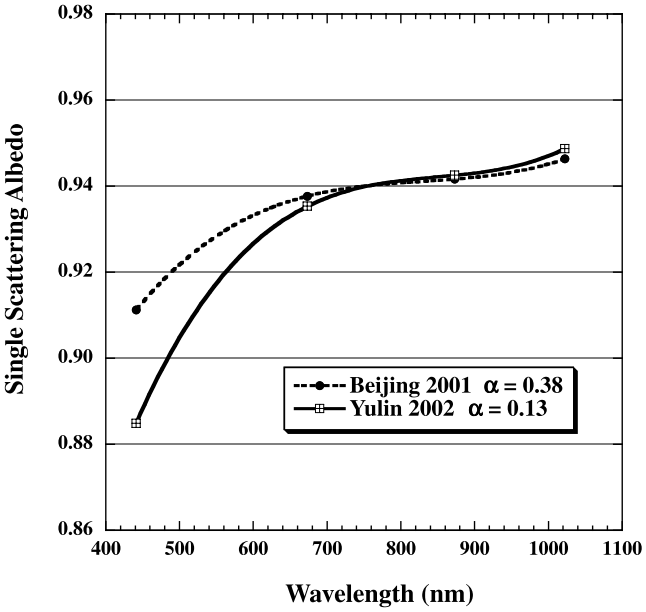

Figure 21. Comparison of aerosol single scattering albedo for dust cases ($\alpha_{440-870} < 0.75$) in Beijing in 2001 and in Yulin, China, in 2002.

shown in this figure are the spectral ω_0 at other globally distributed AERONET sites dominated by dust aerosol as presented in Table 1 of *Dubovik et al.* [2002a]. All of the desert dust spectra presented in Figure 20 are from measurements at high aerosol optical depth (>0.4 at 1020 nm). However, it is noted that there were only 7 good almucantar scans for Dunhuang and only 6 for Anmyon Island in 2001, while Beijing had a much more robust sample of 29 almucantars. The airborne soil dust measured at Dunhuang is relatively close (~550 km east) to the major source region of the Taklamakan Desert basin. The spectral ω_0 measured at Dunhuang are similar to that of Saharan dust measured at Cape Verde for the 675, 870, and 1020 nm wavelengths, but the dust at Dunhuang exhibits less spectral decrease from 675 to 440 nm, possibly due to a lesser iron content in the dust at Dunhuang [*Sokolik and Toon*, 1999]. The ω_0 spectra at Anmyon and Beijing exhibit similar wavelength dependence as observed at Dunhuang but at a lower magnitude, with Beijing (the more polluted site) having the lowest ω_0. This suggests that possibly these differences in ω_0 for the three Asian AERONET sites may be due to dust interaction with pollution, thereby increasing the aerosol absorption [*Huebert et al.*, 2003]. However, there are additional dust sources between the Taklamakan Desert and Beijing (southern Gobi, inner Mongolia, and Mu Us desert); therefore it is possible that dust from these source regions have different absorption properties than from the Taklamakan region. During ACE-Asia in spring 2001, aircraft sampling near Korea and Japan often encountered pure dust in elevated layers, and measurements of dust characterized by coarse mode size and a dust-like chemical signature yielded a mean midvisible (~550 nm) ω_0 of ~0.96 [*Anderson et al.*, 2003]. This value is similar in magnitude to the midvisible ω_0 of ~0.97 retrieved from AERONET measurements in Dunhuang, China, and ~0.95 at Anmyon, South Korea also in spring 2001 (Figure 20).

[37] Desert dust spectral single scattering albedo (measurements where $\alpha_{440-870} < 0.75$) for Beijing in 2001 and for Yulin in 2002 are shown in Figure 21, for retrievals where $\tau_{a1020} > 0.40$. The means of ω_0 shown are from 29 almucantar scans in Beijing and 24 scans in Yulin. Although these data are from different years, this comparison suggests that the coarse mode dominated aerosol cases in both sites (mean $\alpha_{440-870} = 0.38$ for Beijing and = 0.13 for Yulin) have nearly equal single scattering albedo from 675 to 1020 nm, and are nearly constant at ~0.94. The difference between these two sites at 440 nm of ~0.025 may be due to several factors, including possible differences in dust optical properties from a different combination of source regions in different years and possible differences in local fine mode pollution that may interact with the desert dust aerosol, as also suggested by *Alfaro et al.* [2003].

4. Summary and Conclusions

[38] Analysis of spectral aerosol optical depths and AERONET inversion retrievals of column integrated aerosol optical properties over the entire annual cycle were performed for several sites in central eastern Asia and the tropical mid-Pacific (Hawaiian Island chain).

[39] 1. Multiyear monitoring at four Asian sites (Shirahama, Japan; Anmyon Island, South Korea; Beijing, China; Dalanzadgad, Mongolia) show an extremely wide range in aerosol loading, from a yearly mean τ_{a500} of 0.77 at Beijing (city center) to 0.12 at a rural site in southern Mongolia (Dalanzadgad). The annual cycle of monthly mean τ_{a500} at most of these sites suggest a general spring and/or summer maximum and a minimum in winter, although continued monitoring is needed in order to more accurately characterize the annual cycle since only ~2 years of data has been collected at some of these sites.

[40] 2. The annual cycle of monthly mean Angstrom wavelength exponent ($\alpha_{440-870}$) at these same four Asian sites show minimum values in spring (March–May) during this season of maximum dust storm activity. However, the monthly mean minimums of $\alpha_{440-870}$ for all months at all of these sites exceed ~0.80 even in spring, therefore suggesting that while desert dust contributions to total aerosol optical depth are significant, fine mode pollution aerosol contributes more to the optical depth during the entire year at these locations. However, for a site west of Beijing in a more arid region and downwind of major dust sources (Yulin, China), the Angstrom exponent ranged between 0.3 and 0.4 in March and April of 2002, thus dust aerosol strongly dominated the optical depth in spring 2002 in this location.

[41] 3. Multiyear monitoring of aerosol optical depth in the tropical mid-Pacific shows a strong maximum in March–May due to transport of aerosol from Asia eastward in that season. Measurements made at Mauna Loa Observatory at 3.4 km altitude and at Lanai near sea level (~200 km apart but >8000 km from the Asian sources) suggest that ~35% of the springtime enhancement in τ_{a500} is from aerosol above 3.4 km altitude. In 2001, the springtime peak τ_{a500} in April at near sea level in Midway was ~0.21, nearly twice as high as at Lanai (~0.11) since Midway is ~7.5° farther north in latitude and therefore in a zone of stronger eastward transport and also ~2000 km

closer to Asia than Lanai. In the nonspring months of July–December 2001 the τ_{a500} at Midway and Lanai were nearly equal ($\Delta\tau_{a500} < 0.01$).

[42] 4. Column integrated volume size distributions for predominately fine mode aerosol cases ($\alpha_{440-870} > 0.75$) at both Beijing and Anmyon Island exhibited shifts in accumulation mode particle size towards larger particles as τ_a increased. The fine mode particle size at high τ_a at Beijing was not quite as large as at Anmyon, at equal τ_a levels. This may possibly be the result of large daily production of fresh (and therefore smaller) accumulation mode particles in Beijing and also possibly from particle growth through coagulation in cases of aerosol transport from China to the Anmyon site. Additionally, hygroscopic particle growth may be greater at Anmyon due to higher relative humidity when aerosol is transported over the Yellow Sea to the site.

[43] 5. The average aerosol single scattering albedo for fine mode aerosol dominated cases ($\alpha_{440-870} > 0.75$) was similar for two continental sites in China that are in semiarid environments (Yulin and Beijing). The average midvisible (550 nm) ω_0 at these two urban sites was ~0.89. This compares to a mean ω_0 at 550 nm at two relatively rural coastal sites in Japan and South Korea (Shirahama and Anmyon) of ~0.93, again similar at both sites. These differences in absorption between continental urban and coastal rural region pollution aerosol may result from a combination of factors including relative humidity differences, aerosol aging during transport, sea salt at coastal sites, and fuel combustion differences (of both fuel types and combustion technology) in the two regions. Comparison of ω_0 retrieved for Beijing for pollution dominated cases to other major urban centers where AERONET monitoring has occurred (Washington, D. C., Paris, and Mexico City) show the Beijing aerosol to be much more absorbing than in either Washington, D. C., or Paris, but similar to Mexico City. This suggests a much greater contribution of soot or black carbon in the aerosol composition of both Beijing and Mexico City.

[44] 6. Comparison of the single scattering albedo of dust ($\alpha_{440-870} < 0.75$) at the Asian sites of Dunhuang, China in the western desert source region, Beijing, and Anmyon, South Korea in the spring of 2001 showed very similar spectral dependence at all three sites however the ω_0 at Dunhuang was ~0.04 higher than at Beijing at all wavelengths from 440 to 1020 nm, while Anmyon was intermediate in magnitude. This suggests the possible interaction of fine mode pollution aerosol with the coarse mode dust since Beijing has the highest pollution and the lowest dust aerosol ω_0. However, other factors such as varying dust optical properties from dust originating in different source regions may also have contributed to the observed differences in absorption.

[45] **Acknowledgments.** This project was supported by Michael D. King, NASA EOS project office. We thank the AERONET site managers at sites in China (Zhang Jiping – Yulin; Zhang Wenxing - Beijing), South Korea (Byoung-Cheol Choi and Joo-Wan Cha - Anmyon), Japan (Itaru Sano - Shirahama), Mongolia (Hugo S. Khudulmur, Mr. Enkhtuwshin, Mr. Surenjaw, Odbayar Mishigdorj, and Dashjamtsyn Zorig - Dalanzadgad), and the Hawaiian islands (Paul Fukumura-Sawada and Steve Ryan – MLO; Dennis Clark and Mark Yarborough – Lanai; Mike Daak – Midway Island) for maintaining instruments and making the collection of these data possible. We acknowledge the critical efforts of AERONET team members Mikhail Sorokine, Wayne Newcomb, and An Ho in maintaining and adjusting the radiometers deployed in the AERONET network. We also thank the anonymous reviewer for comments that lead to a significant addition to the paper.

References

Ackerman, A. S., O. B. Toon, D. E. Stevens, A. J. Heymsfield, V. Ramanathan, and E. J. Welton (2000), Reduction of tropical cloudiness by soot, *Science*, *288*, 1042–1047.

Alfaro, S. C., et al. (2003), Chemical and optical characterization of aerosols measured in spring 2002 at the ACE-Asia supersite, Zhenbeitai, China, *J. Geophys. Res.*, *108*(D23), 8641, doi:10.1029/2002JD003214.

Anderson, T. L., S. J. Masonis, D. S. Covert, N. C. Ahlquist, S. G. Howell, A. D. Clarke, and C. S. McNaughton (2003), Variability of aerosol optical properties derived from in situ aircraft measurements during ACE-Asia, *J. Geophys. Res.*, *108*(D23), 8647, doi:10.1029/2002JD003247.

Aoki, K., and Y. Fujiyoshi (2003), Sky radiometer measurements of aerosol optical properties over Sapporo, Japan, *J. Meteorol. Soc. Jpn.*, *81*(3), 493–513.

Barnes, J. E., and D. J. Hoffman (1997), Lidar measurements of stratospheric aerosol over Mauna Loa Observatory, *Geophys. Res. Lett.*, *24*, 1923–1926.

Bergstrom, R. W., P. B. Russell, and P. Hignett (2002), Wavelength dependence of the absorption of black carbon particles: Predictions and results from the TARFOX experiment and implications for the aerosol single scattering albedo, *J. Atmos. Sci.*, *59*, 567–577.

Carrico, C. M., P. Kus, M. J. Rood, P. K. Quinn, and T. S. Bates (2003), Mixtures of pollution, dust, sea salt, and volcanic aerosol during ACE-Asia: Radiative properties as a function of relative humidity, *J. Geophys. Res.*, *108*(D23), 8650, doi:10.1029/2003JD003405.

Chameides, W. L., et al. (1999), Case study of the effects of atmospheric aerosols and regional haze on agriculture: An opportunity to enhance crop yields in China through emission controls?, *Proc. Natl. Acad. Sci. U. S. A.*, *96*(24), 13,626–13,633.

Chen, L. L., et al. (1997), Influence of continental outflow events on the aerosol composition at Cheju Island, South Korea, *J. Geophys. Res.*, *102*, 28,551–28,574.

Chin, M., A. Chu, R. Levy, L. Remer, Y. Kaufman, B. Holben, T. Eck, and P. Ginoux (2004), Aerosol distribution in the northern hemisphere during ACE-Asia: Results from global model, satellite observations, and Sun photometer measurements, *J. Geophys. Res.*, *109*, D23S90, doi:10.1029/2004JD004829.

Conant, W. C., J. H. Seinfeld, J. Wang, G. R. Carmichael, Y. H. Tang, I. Uno, P. J. Flatau, K. M. Markowicz, and P. K. Quinn (2003), A model for the radiative forcing during ACE-Asia derived from CIRPAS Twin Otter and R/V *Ronald H. Brown* data and comparison with observations, *J. Geophys. Res.*, *108*(D23), 8661, doi:10.1029/2002JD003260.

Dubovik, O., and M. D. King (2000), A flexible inversion algorithm for the retrieval of aerosol optical properties from Sun and sky radiance measurements, *J. Geophys. Res.*, *105*, 20,673–20,696.

Dubovik, O., A. Smirnov, B. N. Holben, M. D. King, Y. J. Kaufman, T. F. Eck, and I. Slutsker (2000), Accuracy assessments of aerosol optical properties retrieved from AERONET Sun and sky-radiance measurements, *J. Geophys. Res.*, *105*, 9791–9806.

Dubovik, O., B. N. Holben, T. F. Eck, A. Smirnov, Y. J. Kaufman, M. D. King, D. Tanre, and I. Slutsker (2002a), Variability of absorption and optical properties of key aerosol types observed in worldwide locations, *J. Atmos. Sci.*, *59*, 590–608.

Dubovik, O., B. N. Holben, T. Lapyonok, A. Sinyuk, M. I. Mishchenko, P. Yang, and I. Slutsker (2002b), Nonspherical aerosol retrieval method employing light scattering by spheroids, *Geophys. Res. Lett.*, *29*(10), 1415, doi:10.1029/2001GL014506.

Dutton, E. G., P. Reddy, S. Ryan, and J. J. DeLuisi (1994), Features and effects of aerosol optical depth observed at Mauna Loa, Hawaii: 1982–1992, *J. Geophys. Res.*, *99*, 8295–8306.

Eck, T. F., B. N. Holben, J. S. Reid, O. Dubovik, A. Smirnov, N. T. O'Neill, I. Slutsker, and S. Kinne (1999), Wavelength dependence of the optical depth of biomass burning, urban, and desert dust aerosols, *J. Geophys. Res.*, *104*, 31,333–31,349.

Eck, T. F., B. N. Holben, D. E. Ward, O. Dubovik, J. S. Reid, A. Smirnov, M. M. Mukelabai, N. C. Hsu, N. T. O'Neill, and I. Slutsker (2001), Characterization of the optical properties of biomass burning aerosols in Zambia during the 1997 ZIBBEE Field Campaign, *J. Geophys. Res.*, *106*, 3425–3448.

Eck, T. F., B. N. Holben, J. S. Reid, N. T. O'Neill, J. S. Schafer, O. Dubovik, A. Smirnov, M. A. Yamasoe, and P. Artaxo (2003a), High aerosol optical depth biomass burning events: A comparison of optical properties for different source regions, *Geophys. Res. Lett.*, *30*(20), 2035, doi:10.1029/2003GL017861.

Eck, T. F., et al. (2003b), Variability of biomass burning aerosol optical characteristics in southern Africa during the SAFARI 2000 dry season

campaign and a comparison of single scattering albedo estimates from radiometric measurements, *J. Geophys. Res.*, *108*(D13), 8477, doi:10.1029/2002JD002321.

Hansen, J., M. Sato, and R. Ruedy (1997), Radiative forcing and climate response, *J. Geophys. Res.*, *102*, 6831–6864.

Hansen, J., M. Sato, R. Ruedy, A. Lacis, and V. Oinas (2000), Global warming in the twenty-first century: An alternative scenario, *Proc. Natl. Acad. Sci. U. S. A.*, *97*, 9875–9880.

Holben, B. N., et al. (1998), AERONET - A federated instrument network and data archive for aerosol characterization, *Remote Sens. Environ.*, *66*, 1–16.

Holben, B. N., et al. (2001), An emerging ground-based aerosol climatology: Aerosol optical depth from AERONET, *J. Geophys. Res.*, *106*, 12,067–12,097.

Huebert, B. J., T. Bates, P. B. Russell, G. Y. Shi, Y. J. Kim, K. Kawamura, G. Carmichael, and T. Nakajima (2003), An overview of ACE-Asia: Strategies for quantifying the relationships between Asian aerosols and their climatic impacts, *J. Geophys. Res.*, *108*(D23), 8633, doi:10.1029/2003JD003550.

Husar, R. B., J. M. Prospero, and L. L. Stowe (1997), Characterization of tropospheric aerosols over the oceans with the NOAA advanced very high resolution radiometer optical thickness operational product, *J. Geophys. Res.*, *102*(D14), 16,889–16,909.

Intergovernmental Panel on Climate Change (IPCC) (2001), *Climate Change 2001: The Scientific Basis*, edited by J. T. Houghton et al., 896 pp., Cambridge Univ. Press, New York.

Kaufman, Y. J., D. Tanre, and O. Boucher (2002), A satellite view of aerosols in the climate system, *Nature*, *419*(6903), 215–223.

Kim, D. H., B. J. Sohn, T. Nakajima, T. Takamura, T. Takemura, B. C. Choi, and S. C. Yoon (2004), Aerosol optical properties over East Asia determined from ground-based sky radiation measurements, *J. Geophys. Res.*, *109*, D02209, doi:10.1029/2003JD003387.

King, M. D., Y. J. Kaufman, D. Tanre, and T. Nakajima (1999), Remote sensing of tropospheric aerosols from space: Past, present, and future, *Bull. Am. Meteorol. Soc.*, *80*, 2229–2259.

Koren, I., Y. J. Kaufman, L. A. Remer, and J. V. Martins (2004), Measurement of the effect of Amazon smoke on inhibition of cloud formation, *Science*, *303*(5662), 1342–1345.

Kotchenruther, R., and P. V. Hobbs (1998), Humidification factors of aerosols from biomass burning in Brazil, *J. Geophys. Res.*, *103*, 32,081–32,090.

Lee, H. S., C. M. Kang, B. W. Kang, and H. K. Kim (1999), Seasonal variations of acidic air pollutants in Seoul, South Korea, *Atmos. Environ.*, *33*, 3143–3152.

Liu, H. Y., D. J. Jacob, I. Bey, R. M. Yantosca, B. N. Duncan, and G. W. Sachse (2003), Transport pathways for Asian pollution outflow over the Pacific: Interannual and seasonal variations, *J. Geophys. Res.*, *108*(D20), 8786, doi:10.1029/2002JD003102.

Markowicz, K. M., P. J. Flatau, P. K. Quinn, C. M. Carrico, M. K. Flatau, A. M. Vogelmann, D. Bates, M. Liu, and M. J. Rood (2003), Influence of relative humidity on aerosol radiative forcing: An ACE-Asia experiment perspective, *J. Geophys. Res.*, *108*(D23), 8662, doi:10.1029/2002JD003066.

Menon, S., J. Hansen, L. Nazarenko, and Y. F. Luo (2002), Climate effects of black carbon aerosols in China and India, *Science*, *297*(5590), 2250–2253.

Mishchenko, M. I., L. D. Travis, R. A. Kahn, and R. A. West (1997), Modeling phase functions for dustlike tropospheric aerosols using a shape mixture of randomly oriented polydisperse spheroids, *J. Geophys. Res.*, *102*, 16,831–16,847.

Nakajima, T., et al. (2003), Significance of direct and indirect radiative forcings of aerosols in the East China Sea region, *J. Geophys. Res.*, *108*(D23), 8658, doi:10.1029/2002JD003261.

O'Neill, N. T., T. F. Eck, B. N. Holben, A. Smirnov, O. Dubovik, and A. Royer (2001), Bimodal size distribution influences on the variation of Angstrom derivatives in spectral and optical depth space, *J. Geophys. Res.*, *106*, 9787–9806.

Perry, K. D., T. A. Cahill, R. C. Schnell, and J. M. Harris (1999), Long-range transport of anthropogenic aerosols to the National Oceanic and Atmospheric Administration baseline station at Mauna Loa Observatory, Hawaii, *J. Geophys. Res.*, *104*, 18,521–18,533.

Prospero, J. M., D. L. Savoie, and R. Arimoto (2003), Long-term record of nss-sulfate and nitrate in aerosols on Midway Island, 1981–2000: Evidence of increased (now decreasing?) anthropogenic emissions from Asia, *J. Geophys. Res.*, *108*(D1), 4019, doi:10.1029/2001JD001524.

Qiu, J. H. (2003), Broadband extinction method to determine aerosol optical depth from accumulated direct solar radiation, *J. Appl. Meteorol.*, *42*(11), 1611–1625.

Ramanathan, V., and P. J. Crutzen (2003), New directions: Atmospheric brown "clouds,", *Atmos. Environ.*, *37*(28), 4033–4035.

Ramanathan, V., et al. (2001), The Indian Ocean Experiment: An integrated analysis of the climate forcing and effects of the great Indo-Asian haze, *J. Geophys. Res.*, *106*, 28,371–28,398.

Redemann, J., S. J. Masonis, B. Schmid, T. L. Anderson, P. B. Russell, J. M. Livingston, O. Dubovik, and A. D. Clarke (2003), Clear-column closure studies of aerosols and water vapor aboard the NCAR C-130 during ACE-Asia, 2001, *J. Geophys. Res.*, *108*(D23), 8655, doi:10.1029/2003JD003442.

Reid, J. S., P. V. Hobbs, R. J. Ferek, D. R. Blake, J. V. Martrins, M. R. Dunlap, and C. Liousse (1998), Physical, chemical, and optical properties of regional hazes dominated by smoke in Brazil, *J. Geophys. Res.*, *103*, 32,059–32,080.

Reid, J. S., T. F. Eck, S. A. Christopher, P. V. Hobbs, and B. N. Holben (1999), Use of the Angstrom exponent to estimate the variability of optical and physical properties of aging smoke particles in Brazil, *J. Geophys. Res.*, *104*, 27,473–27,489.

Reid, J. S., et al. (2003), Comparison of size and morphological measurements of coarse mode dust particles from Africa, *J. Geophys. Res.*, *108*(D19), 8593, doi:10.1029/2002JD002485.

Satheesh, S. K., and V. Ramanathan (2000), Large differences in tropical aerosol forcing at the top of the atmosphere and Earth's surface, *Nature*, *405*, 60–63.

Schmid, B., J. Michalsky, R. Halthore, M. Beauharnois, L. Harrison, J. Livingston, P. Russell, B. Holben, T. Eck, and A. Smirnov (1999), Comparison of aerosol optical depth from four solar radiometers during the fall 1997 ARM intensive observation period, *Geophys. Res. Lett.*, *26*, 2725–2728.

Schmid, B., et al. (2003), Column closure studies of lower tropospheric aerosol and water vapor during ACE-Asia using airborne Sun photometer and airborne in situ and ship-based lidar measurements, *J. Geophys. Res.*, *108*(D23), 8656, doi:10.1029/2002JD003361.

Seinfeld, J. H., et al. (2004), ACE-Asia - Regional climatic and atmospheric chemical effects of Asian dust and pollution, *Bull. Am. Meteorol. Soc.*, *85*(3), 367–380.

Smirnov, A., B. N. Holben, T. F. Eck, O. Dubovik, and I. Slutsker (2000), Cloud screening and quality control algorithms for the AERONET database, *Remote Sens. Environ.*, *73*, 337–349.

Smirnov, A., B. N. Holben, O. Dubovik, N. T. O'Neill, T. F. Eck, D. L. Westphal, A. K. Goroch, C. Pietras, and I. Slutsker (2002), Atmospheric aerosol optical properties in the Persian Gulf, *J. Atmos. Sci.*, *59*(3), 620–634.

Smirnov, A., B. N. Holben, T. F. Eck, O. Dubovik, and I. Slutsker (2003), Effect of wind speed on columnar aerosol optical properties at Midway Island, *J. Geophys. Res.*, *108*(D24), 4802, doi:10.1029/2003JD003879.

Sokolik, I. N., and O. B. Toon (1999), Incorporation of mineralogical composition into models of the radiative properties of mineral aerosol from UV to IR wavelengths, *J. Geophys. Res.*, *104*(D8), 9423–9444.

Takemura, T., T. Nakajima, A. Higurashi, S. Ohta, and N. Sugimoto (2003), Aerosol distributions and radiative forcing over the Asian Pacific region simulated by Spectral Radiation-Transport Model for Aerosol Species (SPRINTARS), *J. Geophys. Res.*, *108*(D23), 8659, doi:10.1029/2002JD003210.

Tsutsumi, Y., H. Mirishita, M. Yoshida, K. Odashima, A. Saito, K. Suzuki, and O. Ijima (2004), Analyses of aerosol events observed at four Sun photometer sites in Japan during March–April 2002, *J. Meteorol. Soc. Jpn.*, *82*, 1161–1172.

Wolf, M. E., and G. M. Hidy (1997), Aerosols and climate: Anthropogenic emissions and trends for 50 years, *J. Geophys. Res.*, *102*(D10), 11,113–11,121.

Xia, X. A., H. B. Chen, P. C. Wang, X. M. Zong, J. H. Qui, and P. Goloub (2005), Aerosol properties and their spatial and temporal variations over North China in spring 2001, *Tellus, Ser. B*, *57*(1), 28–39.

B. Chatenet, Laboratoire Interuniversitaire des Systèmes Atmosphériques (LISA), Université Paris, 7583 Creteil, France.

H. B. Chen, Institute of Atmospheric Physics, Chinese Academy of Sciences, 100029 Beijing, China.

O. Dubovik, T. F. Eck, D. Giles, B. N. Holben, I. Slutsker, and A. Smirnov, Biospheric Sciences Branch, NASA Goddard Space Flight Center, Greenbelt, MD 20771, USA. (teck@ltpmail.gsfc.nasa.gov)

P. Goloub, Laboratoire d'Optique Amosphérique, Université des Sciences et Technologies de Lille, 59655 Villeneuve d'Ascq, France.

L. Gomes, CNRS, Metéo-France/CNRM/GMEI/MNPCA, 31057 Toulouse, France.

Q. Ji and S.-C. Tsay, Climate and Radiation Branch, NASA Goddard Space Flight Center, Greenbelt, MD 20771, USA.

X.-Y. Zhang, Institute of Earth Environment, Chinese Academy of Sciences, 710075 XiAn, China.